New Phytologist

Research

# Quantifying effects of cold acclimation and delayed springtime photosynthesis resumption in northern ecosystems

**Yunpeng Luo[1,2], Arthur Gessler[1], Petra D'Odorico[1], Koen Hufkens[1,2] and Benjamin D. Stocker[1,2,3,4]**

[1]Swiss Federal Institute for Forest, Snow and Landscape Research WSL, 8903, Birmensdorf, Switzerland; [2]Department of Environmental System Science, Institute of Agricultural Sciences, ETH Zurich, 8902, Zurich, Switzerland; [3]Institute of Geography, University of Bern, Hallerstrasse 12, 3012, Bern, Switzerland; [4]Oeschger Centre for Climate Change Research, University of Bern, Falkenplatz 16, 3012, Bern, Switzerland

Author for correspondence:
*Yunpeng Luo*
*Email: yunpeng.luo@wsl.ch*

Received: *28 January 2023*
Accepted: *24 July 2023*

*New Phytologist* (2023)
**doi**: 10.1111/nph.19208

**Key words:** cold acclimation, eddy covariance, gross primary productivity (GPP), light use efficiency (LUE), photoprotection, photosynthesis modelling, quantum yield, temperate and boreal forests.

## Summary

- Land carbon dynamics in temperate and boreal ecosystems are sensitive to environmental change. Accurately simulating gross primary productivity (GPP) and its seasonality is key for reliable carbon cycle projections. However, significant biases have been found in early spring GPP simulations of northern forests, where observations often suggest a later resumption of photosynthetic activity than predicted by models.
- Here, we used eddy covariance-based GPP estimates from 39 forest sites that differ by their climate and dominant plant functional types. We used a mechanistic and an empirical light use efficiency (LUE) model to investigate the magnitude and environmental controls of delayed springtime photosynthesis resumption (DSPR) across sites.
- We found DSPR reduced ecosystem LUE by 30–70% at many, but not all site-years during spring. A significant depression of LUE was found not only in coniferous but also at deciduous forests and was related to combined high radiation and low minimum temperatures.
- By embedding cold-acclimation effects on LUE that considers the delayed effects of minimum temperatures, initial model bias in simulated springtime GPP was effectively resolved. This provides an approach to improve GPP estimates by considering physiological acclimation and enables more reliable simulations of photosynthesis in northern forests and projections in a warming climate.

## Introduction

Temperate and boreal forests play important roles in regulating global carbon cycle dynamics due to their large spatial coverage (Bradshaw & Warkentin, 2015), their exposure to amplified rates of global warming (Holland & Bitz, 2003; Rantanen *et al.*, 2022), and the large magnitude of the carbon stocks in northern ecosystems (Thurner *et al.*, 2014; Yang *et al.*, 2020). Rapidly increasing temperatures in high latitudes have led to an extension of the growing season (Piao *et al.*, 2019), a widespread increase in active vegetation cover (Keenan & Riley, 2018), and an extension of the carbon (C) uptake season as identified from site-level measurements (Piao *et al.*, 2007; Keenan *et al.*, 2014). However, quantifying changes in biospheric C uptake and modelling terrestrial photosynthesis is particularly challenging for northern ecosystems (Schaefer *et al.*, 2012; Rogers *et al.*, 2017, 2019; Shi *et al.*, 2020; Stocker *et al.*, 2020). Open questions remain regarding the model representation of reductions of photosynthesis in response to very low winter and spring temperatures and the magnitude of related effects on ecosystem fluxes (Schaefer *et al.*, 2012; Rogers *et al.*, 2019). Previous analyses have indicated that systematic model biases persist for photosynthesis simulations in the early growing season for some (but not all) temperate and boreal ecosystems (Schaefer *et al.*, 2012; Shi *et al.*, 2020; Stocker *et al.*, 2020). These biases have implications for the reliability of simulations of the seasonality in ecosystem gross primary production (GPP – the ecosystem-level apparent photosynthesis) and the terrestrial net C balance and affect model predictions of C cycle changes under continued rapid high-latitude warming.

In early spring, the resumption of photosynthetic activity develops with the seasonal increase in solar radiation and temperature. This is governed in deciduous forests by leaf unfolding and the gradual activation of photosynthetic capacity in newly formed leaves (Thomas, 2010; Toomey *et al.*, 2015). In evergreen needleleaf forests, the photosynthetic capacity in existing needles recovers with spring warming (Gamon *et al.*, 2016; Walther *et al.*, 2016). During the early growing season, the trees' carbon assimilation capacity is still low due to not fully expanded leaves in deciduous trees and relatively low concentrations of photosynthetic pigments and maximum quantum yield of photosystem II (PSII) in both deciduous and evergreen trees (Gamon & Surfus, 1999; Jiang *et al.*, 2005). As a consequence, low temperature and excessive irradiance in the early spring during the reactivation of photosynthesis pose a condition where the photosynthetic machinery can be exposed to an imbalance between already significant light energy available for photochemistry, but

limited energy used through $CO_2$ fixation in the Calvin cycle (Huner *et al.*, 1998; Verhoeven, 2014). Such an imbalance arises because low temperatures reduce the rate of enzymatic reactions in the Calvin cycle (Singsaas *et al.*, 2001) more rapidly than they reduce light absorption (Verhoeven, 2014). As a result, the excessive energy can potentially induce light stress and the photosynthetic apparatus (mainly PSII) can be damaged (photodamage) by reactive oxygen species (Huner *et al.*, 1998; Vass, 2012).

To cope with conditions of excess light and low temperatures, many trees, especially evergreens, maintain cold hardiness, which enables them to tolerate adverse growing conditions for photosynthesis by developing photoprotective processes in winter and early spring (Takahashi & Badger, 2011; Hänninen, 2016; Chang *et al.*, 2021). The primary photoprotective mechanism for evergreen trees growing in climates characterized by cold winters is to increase the nonphotochemical dissipation of excessive light as heat (nonphotochemical quenching, NPQ), achieved by an increase in photoprotective pigments (Ensminger *et al.*, 2006; Verhoeven, 2014). Especially, the xanthophyll pool is expanded and most violaxanthin is converted to zeaxanthin with antheraxanthin as the intermediate (Demmig-Adams & Adams, 1996) for sustained quenching while the xanthophyll cycle activity (i.e. the de-epoxidation and epoxidation) is slowed down. This protection mechanism results in a reduction of trees' photochemical efficiency and thus in a reduction of the intrinsic quantum yield of photosynthesis ($\varphi_0$), and their capacity for $CO_2$ assimilation until a gradual relief from reduced efficiency is achieved over the course of spring months (Yang *et al.*, 2020). As a consequence, the recovery of $\varphi_0$ in spring may have a delayed response to rising air temperatures and solar radiation in spring in cold-acclimated trees (Mäkelä *et al.*, 2004; Hänninen, 2016) and they need time to shift the high proportion of photoprotective pigments to a higher proportion of photosynthesis pigments (Ottander *et al.*, 1995; Ensminger *et al.*, 2004). With these processes and the direct mechanistic link between $\varphi_0$ and the ecosystem-level light use efficiency (LUE; Wang *et al.*, 2017; Stocker *et al.*, 2020), substantial photosynthesis reductions in spring can be seen also at the ecosystem level (Mäkelä *et al.*, 2008; Stocker *et al.*, 2020).

Apart from accumulated protective pigments of young leaves (Karageorgou & Manetas, 2006; Ranjan *et al.*, 2014), spring reductions of photochemical efficiency in trees can also be related to hydraulic stress arising from the restricted movement of water in frozen soils and plant tissue and the increasing viscosity of water at low temperatures ('winter drought'; Wang *et al.*, 1992; Charrier *et al.*, 2021; Savage *et al.*, 2022). Hence, due to effects arising from the mechanisms of photoprotection, photodamage, and freezing-related hydraulic stress, reduced springtime photosynthesis and a delayed recovery of $CO_2$ assimilation are expected and can be conceived as a consequence of the plants' exposure and adaptation to very low temperatures during the onset of photosynthetic activity in spring.

Previous studies have emphasized the importance of accounting for the lagged effects of low temperature in photosynthesis models (Mäkelä *et al.*, 2004, 2008; Gea-Izquierdo *et al.*, 2010; Horn & Schulz, 2011). While models are typically formulated using functions of the concurrent climate (Schaefer *et al.*, 2012; Bao *et al.*, 2022b), delayed and slow acclimation to rising temperatures has been recognized to be important for accurately simulating the annual cycle of photosynthesis in ecosystems dominated by evergreen conifers (Bergh *et al.*, 1998; Mäkelä *et al.*, 2008) or in boreal ecosystem across Alaska (Shi *et al.*, 2020). Taking these processes into account can reduce the annual model-based GPP overestimation in coniferous stands in cold regions by up to 40% (Bergh *et al.*, 1998). However, it is not clear to what extent delayed springtime photosynthesis resumption (DSPR) affects carbon fluxes across a wider range of climates, vegetation types, and ecoregions, and what determines the prevalence and magnitude of DSPR across different sites and years.

In addition, it is also not clear to what extent biases in springtime photosynthesis simulations are related to uncertainty in the estimation of canopy structure or physiology. Previous studies have indicated that inaccurate estimates of the fraction of absorbed photosynthetically active radiation (fAPAR) introduce substantial bias in GPP simulations (Zhang, 2021). Light use efficiency models of terrestrial photosynthesis typically use fAPAR estimates, derived from satellite remote sensing data, as a forcing and are thus subject to potential biases. Physiology-related causes for bias in springtime GPP simulations are likely related to $\varphi_0$, which is typically treated as a constant in state-of-the-art Earth System Models and Dynamic Global vegetation models (Rogers *et al.*, 2019). Thus, effects of DSPR are typically ignored. This limits the accuracy of simulations of the seasonal course of C uptake across northern ecosystems, with consequences for their simulated net C balance and atmospheric $CO_2$ seasonality at high northern latitudes – a persistent source of bias in Earth System Models (Graven *et al.*, 2013).

Here, we investigated the DSPR by focussing at the ecosystem-level GPP and LUE and their seasonal course, using data from eddy covariance measurements and remote sensing, and performing empirical and mechanistic modelling. Specifically, we addressed the following questions:

(**1**) What is the prevalence and magnitude of DSPR across sites and years and how does it affect the accuracy of models in simulating seasonal GPP variations?

(**2**) Does springtime GPP bias in model simulations arise due to neglected effects of seasonal climate variations on leaf physiology or due to inaccurate estimates of canopy structure?

(**3**) What are the key environmental factors that control observed patterns of DSPR across sites and years?

(**4**) Does the introduction of a delayed response of $\varphi_0$ to temperature variations in a mechanistic photosynthesis model improve springtime GPP simulations? And can this response be generalized across different plant functional types (PFTs) and climates?

## Materials and Methods

### Site selection and data

To investigate DSPR, we selected 48 forest sites for which eddy covariance (EC) measurements of ecosystem $CO_2$ exchange and simultaneous meteorological variables were available from the FLUXNET 2015 datasets (Pastorello *et al.*, 2020). Sites were

selected, based on their classification into Köppen–Geiger climate classes (Beck *et al.*, 2018), to be located in temperate and cold climates without a dry season (Table 1). This included deciduous broadleaf forest (DBF), mixed deciduous and evergreen needleleaf forest (MF), and evergreen needleleaf forest (ENF; see details in Table 2). EC-based ('observed') daily gross primary production ($GPP_{obs}$) values, obtained through the night-time partition method (Reichstein *et al.*, 2005), were used and data were removed when daytime and night-time partitioned GPP were inconsistent, that is, the upper and lower 2.5% quantiles of the difference between GPP values estimated based on these two methods (Stocker *et al.*, 2020). We aggregated half-hourly meteorological variables to daily values for mean air temperature ($T_{mean}$), maximum air temperature ($T_{max}$), minimum air temperature ($T_{min}$), the daily sum of precipitation (P), mean shortwave incoming radiation ($SW_{IN}$), mean incoming photosynthetically active radiation (PAR), and mean vapour pressure deficit (VPD). Daily soil temperature ($T_{soil}$) and soil water content (SWC) in shallow soil layers (< 30 cm) were also obtained when available. For the comparison of modelled and observed GPP, we removed entire years from the analysis if the time series of $GPP_{obs}$ were not complete in spring and peak seasons (lack of 40% of $GPP_{obs}$ during the period of March–August). Finally, we used a total of 39 sites and 324 site-years to conduct further analyses. Site locations and detailed descriptions can be found in Supporting Information Fig. S1 and Table 2. Remotely sensed estimates of the fraction of absorbed photosynthetically active radiation (fAPAR) were obtained from the Moderate Resolution Imaging Spectroradiometer (MODIS) MCD15A3H Collection 6 product (Myneni *et al.*, 2015), providing observations at 500-m resolution and at 4-d intervals. Data were downloaded for the central pixel, located around the site of ecosystem flux measurements using the MODISTOOLS and INGESTR R packages (Hufkens, 2022; Stocker, 2022). We removed data with poor data quality (i.e. contaminated by cloud or cirrus, shadow, and saturation) and linearly interpolated to daily values. Observed ecosystem LUE was derived from $GPP_{obs}$, PAR, and fAPAR following the LUE model concept (Monteith, 1972):

$$GPP = LUE \cdot fAPAR \cdot PAR \quad \text{Eqn 1}$$

## Identifying the prevalence of DSPR

To identify the prevalence of DSPR, we investigated whether systematic differences in the ecosystem-level LUE and its functional dependencies on environmental covariates could be identified between spring (March–May) vs the remainder of the year, and to what extent low springtime LUE – a reflection of DSPR – caused a systematic overestimation of springtime GPP. Functional dependencies of LUE on concurrent environmental conditions were modelled using a mechanistic and an empirical model with the aim to test whether DSPR is evident based on different methodological approaches.

**Table 1** Description of Köppen–Geiger climate zones and the number of sites for which data are available per climate zone in this study.

| Code | Number | Description |
|---|---|---|
| Cfa | 5 | Warm temperate fully humid with hot summer |
| Cfb | 13 | Warm temperate fully humid with warm summer |
| Dfb | 11 | Cold fully humid with warm summer |
| Dfc | 15 | Cold fully humid with cold summer |

Sites are classified according to Beck *et al*. (2018).

The mechanistic model, the P-model (Wang *et al.*, 2017; Stocker *et al.*, 2020), accounts for the acclimation of LUE to variations in the climate across sites and across months within sites. However, as presented by Stocker *et al.* (2020), the P-model does not account for delayed effects of environmental drivers. The model is formulated as a LUE model (Eqn 1), whereby spatially and seasonally acclimated LUE is predicted based on the Farquhar-von Caemmerer-Berry (FvCB) model for $C_3$ photosynthesis (Farquhar *et al.*, 1980; von Caemmerer & Farquhar, 1981), considering an optimality principle for predicting the trade-off between $CO_2$ assimilation and transpiration (Prentice *et al.*, 2014) and assuming that photosynthetic capacities of the light and the Rubisco-limited assimilation rates are coordinated for average daytime conditions (Maire *et al.*, 2012; Wang *et al.*, 2017). Resulting functional dependencies of photosynthetic capacities, assimilation, and transpiration on monthly average daytime temperature, VPD, light, and $CO_2$ were considered using standard formulations of $C_3$ photosynthesis following the FvCB model (Farquhar *et al.*, 1980; von Caemmerer & Farquhar, 1981) for deriving the optimal, acclimated LUE. Resulting functional dependencies of the P-model to the environment were evaluated by Bloomfield *et al.* (2023). The quantum yield ($\varphi_0$) was modelled as a function of concurrent daily air temperature following the parameterization derived by Bernacchi *et al.* (2003) and $\varphi_0$ linearly scales ecosystem LUE in the P-model (Stocker *et al.*, 2020). A soil moisture stress factor was accounted for in simulations of LUE but affects fluxes only to a minor degree at the sites investigated here. GPP is modelled by the P-model ($GPP_{Pmodel}$) by multiplying simulated LUE with observed fAPAR (see 'Site selection and data' in the Materials and Methods) and PAR following Eqn 1. As a unique feature, compared with other LUE models (Bao *et al.*, 2022b), the P-model predicts LUE variations across sites and across seasons from optimality principles, instead of relying on prescribed and temporally fixed parameters. The coordination hypothesis (Maire *et al.*, 2012; Wang *et al.*, 2017) implies that a linear relationship between incident light and GPP, and between $\varphi_0$ and GPP, arises at weekly-to-monthly time scales (Haxeltine & Prentice, 1996; Wang *et al.*, 2017) and the photosynthesis relations embodied by the FvCB model can thus be written in the form of a LUE model. The P-model should thus provide a basis to account for the acclimation of LUE to average conditions during the growing season (here, considering an average monthly climate), but does not explicitly model effects of cold acclimation and DSPR. For all analyses in this study, we used data published by Stocker *et al.* (2020) as $GPP_{Pmodel}$.

The empirical model is a linear mixed-effects model (LME) with observed ecosystem LUE as the target variable, and $T_{mean}$ and VPD as predictors, fitted to data from nonspring months

**Table 2** Sites used for this analysis.

| Site | Long. | Lat. | Period | Veg. | Clim. | Reference |
|---|---|---|---|---|---|---|
| BE-Vie | 6.00 | 50.31 | 2000–2014 | MF | Cfb | Berbigier *et al*. (2001) |
| CA-Man | −8.48 | 55.88 | 2000–2008 | ENF | Dfc | Dunn *et al*. (2007) |
| CA-NS1 | −98.48 | 55.88 | 2003–2005 | ENF | Dfc | Goulden (2019) |
| CA-NS2 | −98.52 | 55.91 | 2002–2004 | ENF | Dfc | Goulden (2019) |
| CA-NS3 | −98.38 | 55.91 | 2002–2005 | ENF | Dfc | Goulden (2019) |
| CA-NS4 | −98.38 | 55.91 | 2003–2005 | ENF | Dfc | Goulden (2019) |
| CA-NS5 | −98.48 | 55.86 | 2002–2005 | ENF | Dfc | Goulden (2019) |
| CA-Qfo | −74.34 | 49.69 | 2004–2010 | ENF | Dfc | Bergeron *et al*. (2007) |
| CH-Lae | 8.37 | 47.48 | 2005–2014 | MF | Cfb | Etzold *et al*. (2011) |
| CN-Qia | 115.06 | 26.74 | 2003–2005 | ENF | Cfa | Wen *et al*. (2010) |
| CZ-BK1 | 18.54 | 49.50 | 2004–2008 | ENF | Dfb | Acosta *et al*. (2013) |
| DE-Hai | 10.45 | 51.08 | 2000–2012 | DBF | Cfb | Knohl *et al*. (2003) |
| DE-Lkb | 13.30 | 49.10 | 2010–2013 | ENF | Cfb | Lindauer *et al*. (2014) |
| DE-Obe | 13.72 | 50.78 | 2008–2014 | ENF | Cfb | Bernhofer *et al*. (2008–2014) |
| DE-Tha | 13.57 | 50.96 | 2000–2014 | ENF | Cfb | Grünwald & Bernhofer (2007) |
| DK-Sor | 11.64 | 55.49 | 2000–2013 | DBF | Cfb | Pilegaard *et al*. (2011) |
| FI-Hyy | 24.30 | 61.85 | 2000–2014 | ENF | Dfc | Suni *et al*. (2003) |
| FR-Fon | 2.78 | 48.48 | 2006–2013 | DBF | Cfb | Delpierre *et al*. (2016) |
| FR-LBr | −0.77 | 44.72 | 2001–2008 | ENF | Cfb | Berbigier *et al*. (2001) |
| IT-Col | 13.59 | 41.85 | 2001–2014 | DBF | Cfa | Valentini *et al*. (1996) |
| IT-Isp | 8.63 | 45.81 | 2013–2014 | DBF | Cfb | Ferréa *et al*. (2012) |
| IT-Lav | 11.28 | 45.96 | 2013–2014 | ENF | Cfb | Marcolla *et al*. (2003) |
| IT-PT1 | 9.06 | 45.20 | 2003–2004 | DBF | Cfa | Migliavacca *et al*. (2009) |
| IT-Ren | 11.43 | 46.59 | 2002–2013 | ENF | Dfc | Migliavacca *et al*. (2009) |
| JP-MBF | 142.32 | 44.39 | 2004–2005 | DBF | Dfb | Matsumoto *et al*. (2008) |
| JP-SMF | 137.08 | 35.26 | 2003–2006 | MF | Cfa | Matsumoto *et al*. (2008) |
| NL-Loo | 5.74 | 52.17 | 2000–2013 | ENF | Cfb | Moors (2012) |
| RU-Fyo | 32.92 | 56.46 | 2000–2014 | ENF | Dfb | Kurbatova *et al*. (2008) |
| US-GBT | −106.24 | 41.37 | 2002–2003 | ENF | Dfc | Zeller & Nikolov (2000) |
| US-GLE | −106.24 | 41.37 | 2006–2014 | ENF | Dfb | Frank *et al*. (2014) |
| US-Ha1 | −72.17 | 42.54 | 2000–2012 | DBF | Dfb | Urbanski *et al*. (2007) |
| US-MMS | −86.41 | 39.32 | 2000–2014 | DBF | Cfa | Dragoni *et al*. (2011) |
| US-NR1 | −105.55 | 40.03 | 2000–2014 | ENF | Dfc | Monson *et al*. (2002) |
| US-PFa | −90.27 | 45.95 | 2000–2014 | MF | Dfb | Desai *et al*. (2015) |
| US-Prr | −147.49 | 65.12 | 2011–2012 | ENF | Dfc | Nakai *et al*. (2013) |
| US-Syv | −89.35 | 46.24 | 2002–2014 | MF | Dfb | Desai *et al*. (2005) |
| US-UMB | −84.17 | 45.56 | 2000–2014 | DBF | Dfb | Gough *et al*. (2013) |
| US-UMd | −84.70 | 45.56 | 2008–2014 | DBF | Dfb | Gough *et al*. (2013) |
| US-WCr | −90.08 | 45.81 | 2000–2014 | DBF | Dfb | Cook *et al*. (2004) |

Long. is longitude in degrees east. Lat. is latitude in degrees north. Period indicates years for which data were used and included complete spring and peak seasons. Veg. stands for vegetation type: deciduous broadleaf forest (DBF); mixed deciduous and evergreen needleleaf forest (MF); evergreen needleleaf forest (ENF). Clim. indicates the Köppen–Geiger climatic zones (Beck *et al*., 2018), which were described detailed in Table 1.

and multiple sites. Site identity was treated as the grouping variable for the random intercept, and the model was fitted via the restricted maximum likelihood (REML) algorithm using the LME4 R package (Bates *et al*., 2015). Predicted LUE was then used in combination with observed fAPAR and PAR to predict GPP, termed $GPP_{LME}$, following Eqn 1. By fitting the LME model using data outside spring and comparing predicted and observed GPP for all days, we investigated the accuracy and potential bias of the model representing the assumption that GPP can be modelled solely based on concurrent environmental conditions and ignoring effects of DSPR.

To investigate the role of DSPR in affecting the seasonal course of GPP, we aggregated observed and modelled GPP time series, simulated for each day and each site, to mean seasonal cycles by vegetation type and climate zones and compared model bias during spring (March–May) and during the remainder of the year. For a detailed PFT and climate classification of each site (Tables 1, 3).

## Comparing the roles of canopy structure and plant physiology to DSPR

To investigate whether bias in modelled springtime GPP is related to inaccurate representations of canopy structure (expressed by fAPAR) or neglected effects of seasonal climate variations on leaf physiology (expressed by LUE), we analysed the relationship of GPP biases ($GPP_{Pmodel} - GPP_{obs}$ and $GPP_{LME} - GPP_{obs}$) with the magnitude of fAPAR (in 10 equally spaced bins) in different sites and considering the seasonal timing (distinguishing 'springtime', here January to June, and remaining months). If GPP model biases were due to systematic errors in fAPAR, a consistent pattern of the bias in relation to fAPAR

**Table 3** Key acronyms in the manuscript and critical parameters of the cold-acclimated modifier in the model.

| | Symbol | Embedded equation | Meaning | Unit |
|---|---|---|---|---|
| Acronyms | DSPR | – | Delayed spring photosynthesis resumption | |
| | $SY_{DSPR}$ | – | Sites and years where GPP was significantly affected by DSPR | |
| | $SY_0$ | – | Sites and years that were not affected by DSPR | |
| | $GPP_{Pmodel}$ | – | GPP simulated by P-model | $g\,C\,m^{-2}\,d^{-1}$ |
| | $GPP_{LME}$ | – | GPP simulated by linear mixed-effects model | $g\,C\,m^{-2}\,d^{-1}$ |
| | $GPP_{adj}$ | – | GPP simulated by P-model, adjusted after applying the cold-acclimation temperature modifier | $g\,C\,m^{-2}\,d^{-1}$ |
| | LUE | – | Light use efficiency | $g\,C\,m^{-2}\,W^{-1}\,d^{-1}$ |
| | $\varphi_0$ | – | Intrinsic quantum yield | |
| | fAPAR | – | Fraction of absorbed photosynthetically active radiation | |
| Parameters in cold-acclimation modifier | $f_T$ | Eqn 3 | Cold-acclimation temperature modifier | |
| | $\tau$ | Eqn 6 | Time constant of the delay for cold-acclimation relief | d |
| | $X_0$ | Eqn 5 | Temperature threshold above which acclimation is initialized | °C |
| | $S_{max}$ | Eqn 4 | Temperature threshold above which photosynthesis is not limited by low temperature | °C |

should emerge across sites and should be quantitatively similar when having the same levels of fAPAR in springtime and the remaining months (e.g. during senescence period). Systematic errors related to fAPAR may also be reflected by patterns in the GPP model bias relating to canopy structural characteristics (broadleaved vs needle-leaved trees). In contrast, if GPP model biases were due to DSPR effects on LUE, a pattern of the bias in relation to the seasonal timing should emerge and may not be equally strong across sites, subject to the varying influence of DSPR effects in different climates and vegetation types.

## Identifying environmental drivers of DSPR

To identify environmental drivers of DSPR across different sites and years, we first developed a binary classification, defining a set of sites and years where GPP was significantly affected by DSPR ($SY_{DSPR}$) and a set of the remaining sites and years where it was not affected by DSPR ($SY_0$). The following procedure was applied to determine $SY_{DSPR}$ and $SY_0$.

(**1**) We normalized the $GPP_{obs}$ and $GPP_{Pmodel}$ time series (yielding $GPP_{obs}'$ and $GPP_{Pmodel}'$) based on their 95$^{th}$ percentile (peak season values), separately at each site. We then extracted different phenophases as the start of the season (SOS), peak of the season (POS), and end of the season (EOS), and defined a 'photosynthesis resumption period' (PRP: between SOS and POS) at each site and in each year using the $GPP_{Pmodel}'$ time series (Fig. S2). These phenological phases were determined based on the smoothed (spline) $GPP_{Pmodel}'$ (Migliavacca *et al.*, 2011; Luo *et al.*, 2018). Peak of the season was defined as the timing (day) of maximum GPP. Start of the season and EOS were defined as the day when the threshold, defined by 10% of the amplitude in $GPP_{Pmodel}$ (maximum − minimum GPP), was crossed. We used $GPP_{Pmodel}$ instead of $GPP_{obs}$ to extract the phenophases to capture the full period with apparent effects of DSPR, including the (sometimes) premature simulated onset of photosynthetic activity in $GPP_{Pmodel}$.

(**2**) We then calculated the bias in normalized modelled GPP ($GPP_{Pmodel}' - GPP_{obs}'$) and, using only data outside the PRP, we fitted a Gaussian normal distribution ($\mu$, $\sigma$) of the bias values. We expect that outside the photosynthesis resumption period, the simulated GPP seasonality is accurate (zero mean of bias values), but affected by the effects of DSPR during the PRP, leading to systematic bias. Using normalized values assured that we considered only bias in the seasonal course, but not bias in magnitudes (constant scaling or offsets). Finally, the set of days $D_{DSPR}$ was defined as days ($d$) during the PRP ($D_{PRP}$) for which biases in $GPP_{Pmodel}'$ were higher than $3\sigma$, where $\sigma$ is determined on bias values outside the PRP (Eqn 2):

$$D_{DSPR} = d \mid d \in D_{PRP} \cap GPP_{Pmodel}'(d) - GPP_{obs}'(d) > 3\sigma \quad \text{Eqn 2}$$

(**1**) We identified the set of site-years $SY_{DSPR}$ (not all years for a certain site were belonging to $SY_{DSPR}$) based on whether they contained days belonging to $D_{DSPR}$ in each specific site-year. All remaining site-years were classified as $SY_0$.

(**2**) Given the binary classification of sites and years into $SY_{DSPR}$ and $SY_0$, we investigated different environmental covariates among the two classes. For this, we separately aligned data of $SY_{DSPR}$ and $SY_0$ with respect to the first day of the PRP and aggregated data by taking the mean across sites and years for each 'photosynthesis resumption day' (day after the start of the photosynthesis resumption period). The comparison was focussed on the period between 60 d before the PRP and the end of the period when GPP was overestimated in $SY_{DSPR}$. We selected 60 d as a conservative threshold because previous studies indicated the green-up of vegetation is most correlated with environmental drivers such as temperature and precipitation occurring 2–3 months (Cong *et al.*, 2013; Guo *et al.*, 2020). For $SY_0$, the same resumption day-specific aggregation across sites and years was performed.

### Modelling DSPR effects on GPP

To account for DSPR effects on GPP in the ecosystem-level photosynthesis model, we assumed that a delayed resumption of ecosystem LUE (Eqn 1) is attributed to a lagged response of the quantum yield ($\varphi_0$) to temperature increases in early spring. By assuming that the lagged photosynthesis recovery arises through effects that are expressed in $\varphi_0$, we can make use of the linear relation between the acclimated LUE and $\varphi_0$ in the P-model (Stocker *et al.*, 2020) and introduce a multiplicative cold-acclimation temperature modifier ($f_T$), directly multiplying LUE and hence GPP simulated by the P-model ($GPP_{Pmodel}$). We thus obtain the adjusted GPP ($GPP_{adj}$; Eqn 3) as:

$$GPP_{adj} = f_T GPP_{Pmodel} \quad \text{Eqn 3}$$

The modifier $f_T$ accounts for the temperature acclimation and a delayed resumption of GPP in response to seasonal temperature variations (Eqns 4–6) following Mäkelä *et al.* (2008):

$$f_{T,t} = \min\left(\frac{S_t}{S_{max}}, 1\right) \quad \text{Eqn 4}$$

$$S_t = \max(X_t - X_0, 0) \quad \text{Eqn 5}$$

$$X_t = X_{t-1} + \frac{1}{\tau}(T_{min,t} - X_{min,t-1}) \quad \text{Eqn 6}$$

where $T_{min,t}$ (°C) is the daily minimum air temperature of day $t$. In the original model formulation, Mäkelä *et al.* (2008) used the daily mean air temperature ($T_{mean}$). We used $T_{min}$ as we found that $T_{min}$ is more relevant to the GPP recovery in spring compared with $T_{mean}$ after comparing the environmental covariates between $SY_{DSPR}$ and $SY_0$ in 'Comparing the roles of canopy structure and plant physiology to DSPR' in the Materials and Methods. $X_t$ is the delayed minimum air temperature and is computed using a first-order dynamic delay model that is driven by concurrent $T_{min,t}$ and $X_{t-1}$, the value on the preceding day $(t-1)$. The parameter $\tau$ (expressed in days) is the time constant of the delay process, which represents the rate of change in trees' acclimation state (Mäkelä *et al.*, 2004, 2008). $S_t$ (°C) is the state of acclimation that depends on the minimum temperature threshold $X_0$ (°C). Above this threshold, $f_T$ is higher than 0. $S_{max}$ (°C) is the minimum temperature threshold at which photosynthesis is not inhibited by low temperatures (Tian *et al.*, 2020, 2021). Above this threshold, $f_T$ is 1.

We also tested an alternative approach to implementing the cold-acclimated temperature modifier as detailed in Notes S1. This had a similar performance compared with the above approach.

### Model calibration and evaluation

Parameters determining the cold-acclimation modifier $f_T$ ($\tau$, $X_0$, $S_{max}$; Table 3) were calibrated to minimize the mean square error (MSE) between daily $GPP_{adj}$ and $GPP_{obs}$. To test the generality of the $f_T$ model and its parameterization, we performed calibrations at different levels. First, we calibrated the parameters separately for each site. Second, we calibrated parameters separately for each PFT. Third, we calibrated a single set of parameters, fitted for all sites simultaneously. Given the parameter sets obtained at the different levels of calibration, we investigated differences in calibrated parameters across sites, and across PFTs. We also performed an analysis of the relationship between fitted parameter values and environmental drivers across different sites.

Parameters in Eqns 4–6 were calibrated (5000 iterations for each calibration level) by using the generalized simulated annealing method implemented in the GENSA R package (Xiang *et al.*, 2013). Results were evaluated by calculating mean bias, mean absolute error (MAE), the coefficient of determination ($R^2$), and the root mean square error (RMSE) between $GPP_{adj}$ and $GPP_{obs}$ for all sites' data pooled and for simultaneous distinction of climate zones and vegetation types ('Clim-PFTs').

## Results

### Identifying the prevalence of DSPR

We compared the mean seasonal cycle of observed and modelled GPP, where model results were based on the P-model without the cold-acclimation modifier and the empirical LUE models (Figs 1, S3). The results from the empirical (LME) LUE model conform to the results from the mechanistic (P-model) LUE models. While most of the peak season, autumn, and winter GPP were simulated accurately across a wide range of climate and vegetation types, a systematic positive bias in early spring was often evident in both modelling approaches. This early season bias was found in all PFTs and was most evident in sites with deciduous broadleaved vegetation (Figs 1, S3) of the temperate climate zones Cfa and Cfb and in the boreal climate zone Dfb, where an early season GPP bias was found for all vegetation types.

Similar patterns were found for modelled and observational LUE (Fig. S4), derived from observed PAR and fAPAR using Eqn 1. For all boreal sites (Dfb and Dfc), a positive model bias was found for the early season, but not for the late season. A distinct seasonal course with low observation-based LUE estimates during winter was not captured by the model.

We also found a geographic pattern in the prevalence of DSPR effects. The springtime GPP overestimation is most clearly evident for North American sites, while springtime GPP overestimation was variable for European sites, and less evident for two Japanese sites (Fig. 2a). The widespread positive springtime model bias is indicative of the importance of the DSPR effect in many, but not all climates and was similarly expressed in different vegetation types (Fig. 2b).

### Comparing the roles of canopy structure and plant physiology in driving GPP model bias

Across different vegetation types and climate zones, we found that GPP is often overestimated at low and intermediate fAPAR during months between January and June but no general overestimation

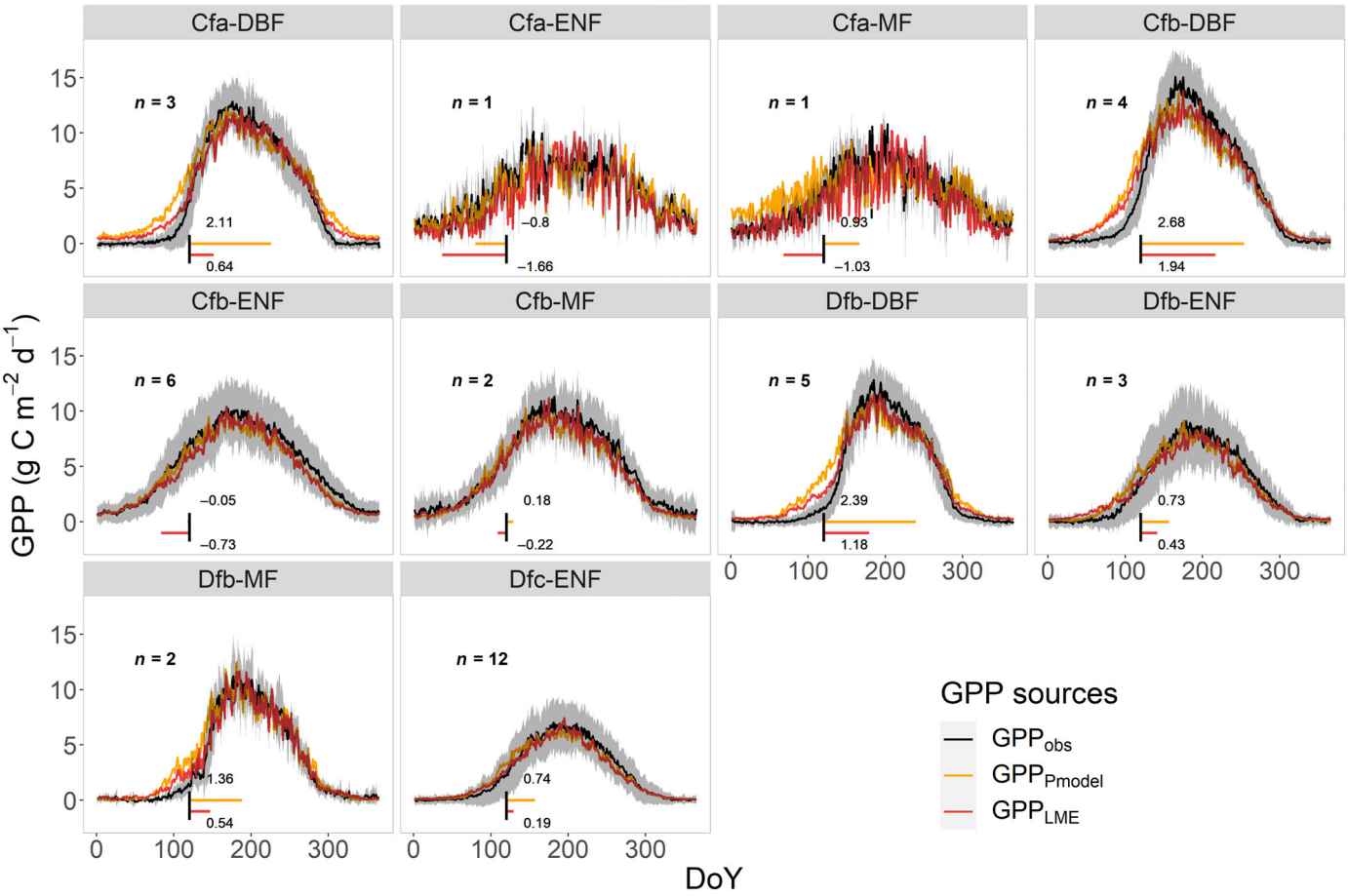


**Fig. 1** Comparison of the mean seasonal cycle of GPP among different data sources: P-model ($GPP_{Pmodel}$), linear mixed-effects regression LUE model ($GPP_{LME}$), and EC-based (observation-based) GPP ($GPP_{obs}$) across 10 different combinations of Köppen–Geiger climate zones (Table 1) and plant functional types. The grey bands represent the range of mean ± SD of $GPP_{obs}$ for each day of the year (DoY). Different PFTs are as follows: deciduous broadleaf forest (DBF); mixed deciduous and evergreen needleleaf forest (MF); and evergreen needleleaf forest (ENF). The horizontal lines (the length of lines was proportionally magnified for the purpose of visualization) and values at bottom of each panel indicate the mean GPP bias (g C $m^{-2}$ $d^{-1}$) between modelled GPP ($GPP_{Pmodel}$ and $GPP_{LME}$) vs $GPP_{obs}$ during the photosynthesis resumption period. The number of sites (*n*) from which data are aggregated within each panel (climate zone and PFT) is listed inside each panel.

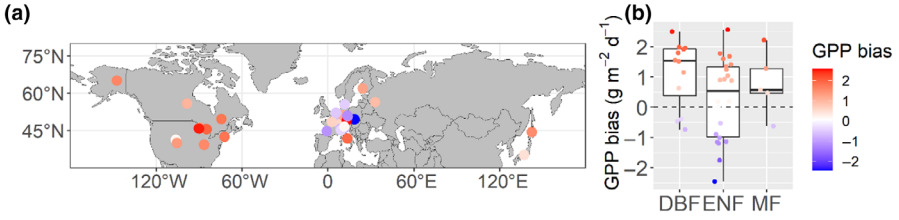


**Fig. 2** Sites selected for the analysis and their mean GPP bias ($GPP_{Pmodel} - GPP_{obs}$ difference between modelled GPP by P-model ($GPP_{Pmodel}$) and 'observed' GPP from eddy covariance tower ($GPP_{obs}$)) during photosynthesis resumption period: (a) locations of studied sites and their mean GPP bias and (b) variations of the GPP bias among different plant functional types. DBF, deciduous broadleaf forest; ENF, evergreen needle-leaved forest; MF, mixed deciduous and evergreen forest. The length of each box indicates the interquartile range, and the horizontal line inside each box represents the median. The lower and upper lines extending from boxes correspond to the quartiles plus 1.5 times the interquartile range. Additional information on the sites is listed in Table 2.

or underestimation is apparent at low fAPAR later in the year. Similar patterns emerge for bias in the P-model (Fig. 3) and in the LME model (Fig. S5). Corresponding visualizations for each site are given in Figs S6, S7. The seasonal discrepancy was most clearly expressed in sites belonging to the Cfb-DBF and all Dfb and Dfc groups. No clear difference in the bias of GPP simulated by the P-model was found between different vegetation types and different canopy structural properties (Fig. 2b). We also found a general tendency of the LME model and the P-model to underestimate GPP when fAPAR was high. However, this aspect of model biases is not relevant in the context of the DSPR (fAPAR is generally low in the early season).

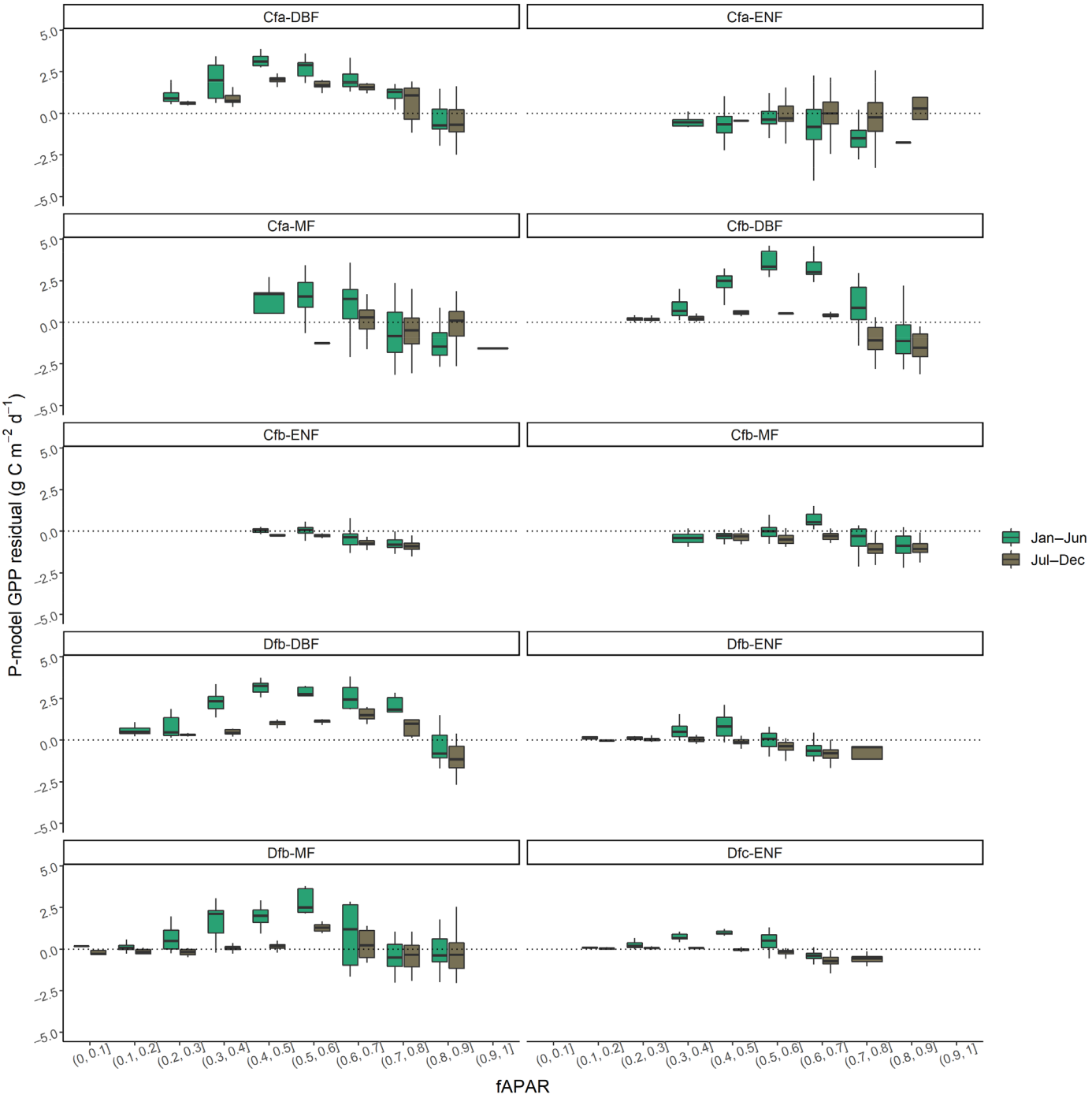


**Fig. 3** Bias in GPP simulated by the P-model within bins of the fraction of absorbed photosynthetically active radiation (fAPAR) and separated into the early and late seasons of northern ecosystems. 'Jan–Jun' contains data from months January–June, while 'Jul–Dec' contains data from months July–December. Panels separate data by different vegetation and climate zones. Different PFTs are as follows: deciduous broadleaf forest (DBF); mixed deciduous and evergreen needleleaf forest (MF); evergreen needleleaf forest (ENF). Different Köppen–Geiger climate zones can be referred in Table 1. The length of each box indicates the interquartile range, and the horizontal line inside each box represents the median. The lower and upper lines extending from boxes correspond to the quartiles plus 1.5 times the interquartile range.

## Identifying drivers of DSPR

Sites and years where effects of DSPR were identified ($SY_{DSPR}$) were characterized by higher incident radiation throughout and before the photosynthesis resumption period (PAR; Fig. 4b), while $T_{min}$ was distinctively lower compared with sites and years in $SY_0$, especially before the photosynthesis resumption period (Fig. 4c). No clear differences in the snow fraction were found between $SY_{DSPR}$ and $SY_0$ (Fig. 4d). However, a higher snow cover fraction was found in evergreen and mixed forests (Fig. S8b). Besides, data in $SY_{DSPR}$ were characterized by lower soil water content compared with data in $SY_0$, especially in days

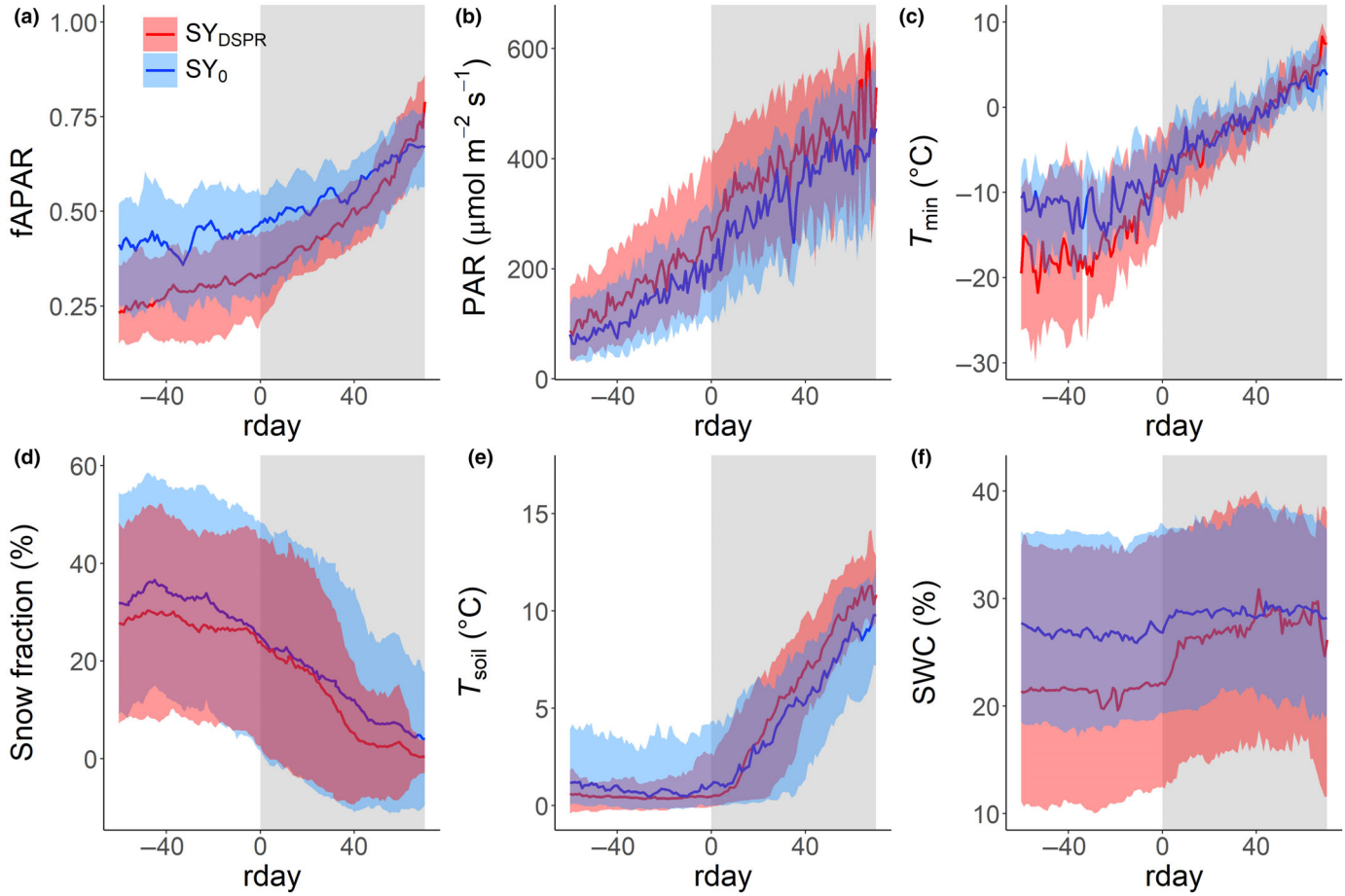


**Fig. 4** Comparison of environmental drivers between the sites and years where GPP was significantly affected by delayed springtime photosynthetic resumption (DSPR; $SY_{DSPR}$; 191 site-years) and the other sites and years where it was not affected by DSPR ($SY_0$; 133 site-years). The data are aligned by the onset of the photosynthesis resumption period (rday), where rday = 0 refers to the first day into the photosynthetic resumption period. Panels are given for (a) fraction of absorbed photosynthetically active radiation (fAPAR), (b) photosynthetically active radiation (PAR), (c) minimum air temperature ($T_{min}$), (d) snow fraction obtained from MODIS MOD10A1 data product, (e) soil temperature ($T_{soil}$), and (f) the volumetric soil water content (SWC). The photosynthesis resumption period is indicated by the shaded area. For (a–c, e, f): lines represent the median, and colour-shaded areas around lines represent the upper and lower 25% quantiles of data aggregated across all years and sites pooled within the $SY_{DSPR}$ or $SY_0$ groups. For (d): the lines stand for the mean, and the shaded area represents the mean ± SD of snow fractions across all years and sites pooled within the $SY_{DSPR}$ or $SY_0$ data subset.

and months before the photosynthesis resumption period. No clear differences in soil temperature and the timing of soil temperature increase were observed between data in $SY_{DSPR}$ and $SY_0$ (Fig. 4e). The fraction of absorbed photosynthetically active radiation (fAPAR) was lower in sites and years where effects of DSPR were identified ($SY_{DSPR}$ in Fig. 4a). However, when separately looking at different vegetation types, fAPAR was higher in deciduous forests, but lower in evergreen needle-leaved and mixed forests for $SY_{DSPR}$, compared with $SY_0$ (Fig. S8).

Temperature and incoming solar radiation are mechanistically related (higher air temperatures when radiation is high), but their divergence (high radiation and low temperature) may induce stress, leading to downregulation or damage to the photosynthetic apparatus. To reveal their interactive effects and the link with the apparent model bias, we further compared the $T_{min}$ between $SY_{DSPR}$ and $SY_0$ within different bins of radiation ($SW_{IN}$ and PAR) between 60 d before the photosynthesis resumption period and the end of the 'overestimated' period (Figs S9, S10). $SY_{DSPR}$ generally has lower $T_{min}$ compared with $SY_0$ for a given level of radiation. This is particularly evident for ENF.

## Model improvement and variation of calibrated parameters

Applying the cold-acclimation temperature modifier $f_T$ to $GPP_{Pmodel}$ improved the model performance when parameters were calibrated at all three different levels (Table 4; Fig. S11). After applying site-specific parameters, the $R^2$ of pooled daily observations and P-model predictions increased from 0.70 to 0.80, while the MAE and RMSE decreased compared with the original model. Analogously, modelled GPP with PFT-specific parameters or with a single set of parameters also improved the $R^2$ to 0.76 and 0.73, respectively (Table 4; Fig. S11). Considering the seasonal cycle of GPP in different climate zones and plant functional types (Clim-PFTs), model improvement was evident when applying calibrated parameters obtained from the calibration done at different levels (Figs 5, S11–S13). The performances of the P-model calibrated with site-specific parameters and with

**Table 4** Model evaluation between $GPP_{Pmodel}$ and $GPP_{adj}$ against $GPP_{obs}$ for calibrations performed at the site level ('site-specific calibration'), PFT level ('PFT-specific calibration'), and using all sites pooled ('general calibration').

| | MAE ($g\,C\,m^{-2}\,d^{-1}$) | RMSE ($g\,C\,m^{-2}\,d^{-1}$) | $R^2$ |
|---|---|---|---|
| $GPP_{Pmodel}$ | 1.6 | 2.3 | 0.70 |
| $GPP_{adj}$ with site-specific calibration | 1.2 | 1.9 | 0.80 |
| $GPP_{adj}$ with PFT-specific calibration | 1.4 | 2.1 | 0.76 |
| $GPP_{adj}$ with a general calibration | 1.5 | 2.2 | 0.73 |

Data were pooled for all sites and days.

PFT-specific parameters were similar, particularly for the most widespread DBF and ENF sites. In contrast, P-model with a single set of parameters performed worse compared with P-model with site or PFT-specific parameters regarding to capture the seasonal changes of GPP. The PFT-specific calibration yielded GPP estimates that were clearly improved, especially when considering the mean seasonal GPP cycle in cold climates (Dfb and Dfc; Fig. 5) and for DBF in temperate climates (Cfa and Cfb; Fig. 5).

Results of the site-level parameterization showed that the fitted parameter values for $\tau$, $X_0$, and $S_{max}$ tended to be smaller (faster acclimation rate, lower temperature threshold for initiation of acclimation, and lower temperature upper limit for inhibiting photosynthesis) for ENF than for DBF (Fig. 6). In contrast, among the few MF sites, we found a large variation in calibrated parameters without a clear pattern. The PFT-level parameters in DBF and ENF generally have a consistent pattern compared with site-level parameters, but the means of the site level were different from the PFT-level parameters. Similarly, the parameters for MF had a large variation and did not have a clear linkage with the ones in DBF and ENF (Fig. 6).

We further compared the calibrated parameters from the site-level calibration with the variation of $T_{min}$ during the period between 60 d before the start of photosynthesis resumption period and peak of the GPP (Fig. 7). We found no significant relationship between parameters and $T_{min}$ in different PFTs (Fig. 7). However, a positive, albeit nonsignificant relationship emerged between $\tau$ and $T_{min}$ for DBF and ENF sites in boreal climates (Dfc-ENF). We also analysed relationships between fitted parameters and other environmental variables, but found no consistent patterns (not shown).

Mean springtime $f_T$ provides a quantification of the DSPR effect across sites (Fig. 8a). As a consequence of the model formulation ($f_T$ being a function of delayed minimum temperatures), the largest GPP reductions (lowest mean $f_T$) were simulated for sites with lowest winter-mean $T_{min}$ (mean $T_{min}$ over months December–February), with mean $f_T$ values in different vegetation types *c.* 0.3–0.5, indicating a 50–70% reduction of GPP, at the coldest sites. The introduction of the cold-acclimation modifier in the model resolves the springtime GPP bias across sites and across the full range of mean winter $T_{min}$ (Fig. 8b,c).

## Discussion

### Evident DSPR in forests with cold winters

The comparisons between $GPP_{obs}$ and simulated GPP from mechanistic and empirical models (i.e. $GPP_{Pmodel}$ and $GPP_{LME}$) indicated that the DSPR phenomenon happens in different vegetation types (Fig. 2b). Effects of DSPR were more clearly evident in North American sites (Fig. 2a) and were especially evident in climates that are characterized by cold winters and low minimum temperatures during the springtime vegetation green-up period (Fig. 4). These results indicate that LUE is depressed in the early spring in forests with cold winters. This depression of LUE in early spring is corroborated by previous studies on plant physiology, which found that PSII photochemical efficiency reached a minimum in late winter and was depressed until late spring (Ottander *et al.*, 1995; Ensminger *et al.*, 2004; Zarter *et al.*, 2006).

We found that spring GPP can be overestimated by up to 30–70% (Fig. 8) due to a lack of considering DSPR effects in models. This magnitude of overestimation is comparable to a previous study conducted in a boreal forest (Bergh *et al.*, 1998), but the estimated magnitudes here are representative for 39 sites, distributed across the boreal and temperate zones, and distributed across three continents. Even though the introduction of the cold-acclimated temperature modifier in the model largely resolved the springtime GPP bias across sites when using site-specific parameters, no obvious relationship between site-specific parameters and environmental drivers was found (Fig. 7), and the single general calibrated parameter set only partly removed biases (Table 4). This indicates a remaining challenge in modelling DSPR effects on GPP across diverse biomes and ecosystems with a single generalized model.

### The bias in springtime GPP simulations is due to neglected effects on photosynthesis

Our results indicate that DSPR effects are mainly linked to plant physiology, not to canopy structure or fAPAR inaccuracies (Figs 3, S5–S7). No general relationship was found between the GPP bias and the magnitude of fAPAR across sites, neither for the bias of the mechanistic model nor for the bias of the empirical model. For the sites with DSPR, the GPP bias was evident only for springtime months, but not for summer and autumn months. In contrast, no evident seasonal GPP bias was found under different fAPAR bins at other sites without DSPR (Figs S6, S7). These results indicate that the occurrence of DSPR is independent of the magnitude of fAPAR and should be mainly related to depressed LUE at certain sites (but not at others).

Previous studies have indicated that the satellite remote sensing-derived MODIS fAPAR data can be overestimated as it also includes absorption by nonphotosynthetic tissues, for example stems and branches. These nonphotosynthetic tissues' contributions to the overestimation of fAPAR are not uniform throughout seasons in deciduous forests (Zhang, 2021), but particularly expressed under conditions of low foliage cover.

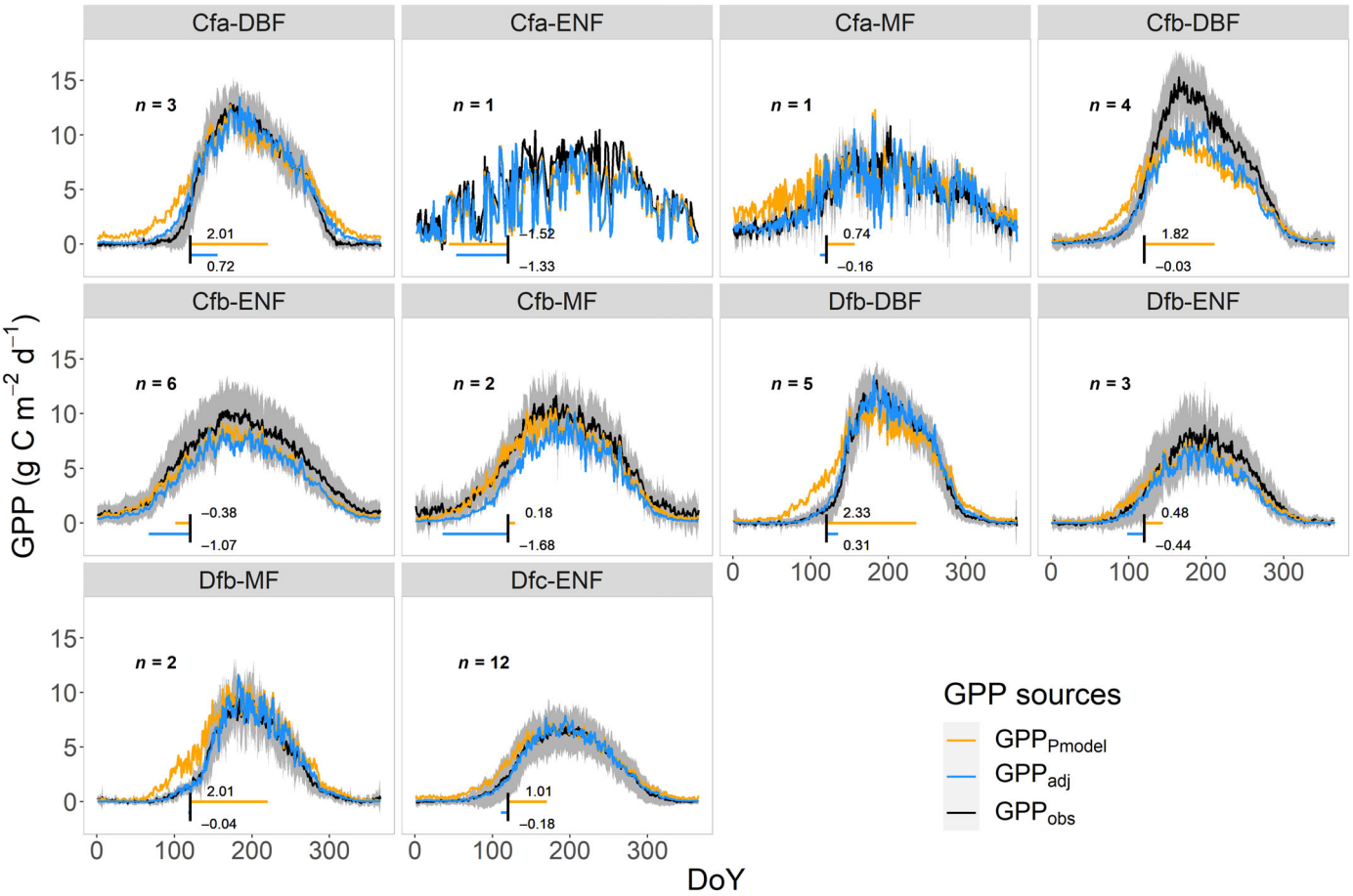


**Fig. 5** Mean seasonal cycle of 'Observed' GPP ($GPP_{obs}$) and modelled GPP from the original P-model ($GPP_{Pmodel}$) and from the adjusted GPP ($GPP_{adj}$) after applying a cold-acclimation temperature modifier ($f_T$) to $GPP_{Pmodel}$, obtained from the PFT-specific calibrations. The data are separated for different combinations of climate zones and PFTs. The grey bands represent the range of mean ± SD of $GPP_{obs}$. The horizontal lines (the length of lines was proportionally magnified for the purpose of visualization) and values at bottom of each panel indicate the GPP bias (g C $m^{-2}$ $d^{-1}$) between modelled GPP and $GPP_{obs}$ during the photosynthesis resumption period. The number of sites (*n*) used for from which data are aggregated within each panel is listed within each panel. DoY, day of the year.

Absorption by nonphotosynthetic tissue should translate into a positive bias in simulated GPP when affected fAPAR estimates are used as inputs in models (Cheng *et al.*, 2006; Zhang *et al.*, 2006). However, such an overestimation of fAPAR should lead to a similar pattern of GPP bias in spring and autumn when fAPAR changes from low to high levels and should be similarly expressed across sites with deciduous vegetation. This, however, was not the case (Figs 3, S3). In addition, snow could also impact fAPAR estimation (Zhang *et al.*, 2006; Zhang, 2021). However, snow presence, which should be more common at sites with cold winters, would generally lead to an underestimation of fAPAR (Moody *et al.*, 2007; Zhang, 2021), and thus to an underestimation of GPP, which cannot explain the DSPR phenomenon we observed here at sites with cold winters. Based on the above reasons, we conclude that lagged effects of low temperatures in preceding days and weeks depress the LUE in spring, but not in autumn (Ensminger *et al.*, 2004; Mäkelä *et al.*, 2008) and lead to GPP model bias in spring, when effects of DSPR are not accounted for in simulations.

Although we argue that errors in fAPAR data used here are not the main cause for the springtime model biases and DSPR we found at certain sites, we recognize that an overestimation of satellite data-derived fAPAR estimates may contribute to an overestimation of GPP simulations. Measured fAPAR from EC sites as well as a better estimate of the radiation absorbed from nonleaf components through more sophisticated radiative transfer models (Zhang *et al.*, 2020; Zhang, 2021) will help to mitigate this limitation.

Systematic model bias with a relation to seasonal changes may also arise by simplifications of the representation of photosynthesis and how it is affected by canopy structure applied in the model here. Canopy-level LUE may increase with the increase in the ratio between shade leaves and sunlit leaves during leaf expansion (Bao *et al.*, 2022a). Separately treating light use efficiency in sunlit and shaded leaves can potentially improve the LUE and GPP estimation in future studies (Wang & Leuning, 1998). However, as argued above, a systematic bias of simulated LUE in relation to seasonal changes in canopy development should lead to a similar pattern of GPP bias with fAPAR variations in spring and autumn and should be similarly expressed across sites with deciduous vegetation. This was, however, not the case.

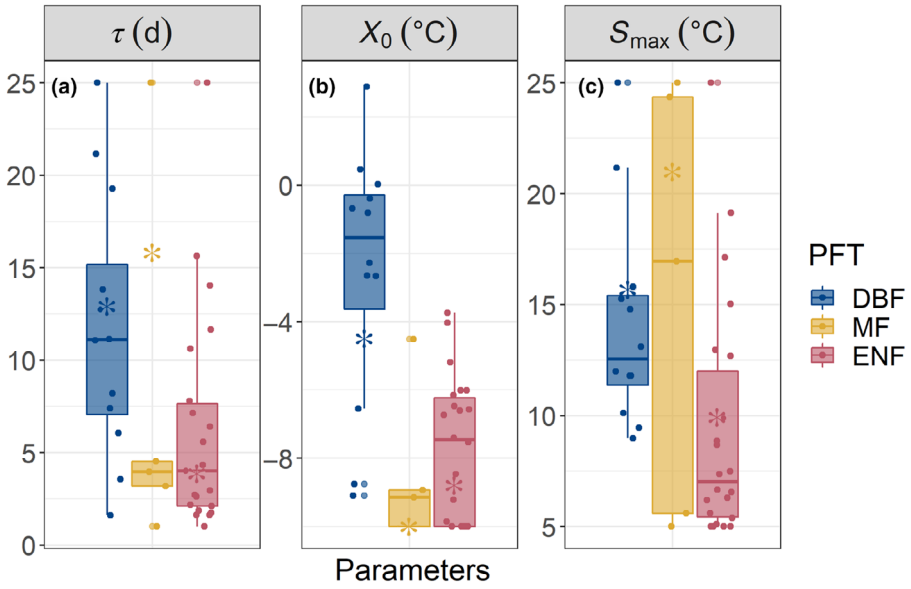


**Fig. 6** Variation of calibrated parameters of the cold-acclimation temperature modifier embedded into the P-model for the different parameters: (a) parameter $\tau$, (b) parameter $X_0$, and (c) parameter $S_{max}$. The site-level calibrated parameters are displayed as points and their variation range is shown by boxplots, grouped by different plant functional types (PFTs). The PFT-level calibrated parameters are displayed as asterisks. DBF, deciduous broadleaf forest; ENF, evergreen needleleaf forest; MF, mixed deciduous and evergreen needleleaf forest. The length of each box indicates the interquartile range, and the horizontal line inside each box represents the median. The lower and upper lines extending from boxes correspond to the quartiles plus 1.5 times the interquartile range. The points outside the extending lines represent outliers.

## Low temperature and high radiation cause GPP biases in spring

The sites and years where and when biases in modelled GPP occurred in spring are characterized by a combination of low minimum temperatures and relatively high radiation during the period of the late winter to early spring (Figs 4, S8). These environmental conditions most likely induce photoprotection processes, with increases in photoprotective pigments and cryoprotective compounds such as soluble sugars (Ottander *et al.*, 1995; Ensminger *et al.*, 2004; Chang *et al.*, 2021), which downregulate plants' photochemical efficiency and dissipate excessive light as heat (Huner *et al.*, 1998; Verhoeven, 2014). Damage accompanied by losses of chlorophylls and D1 protein of the photosystem II (PSII) reaction centre should be avoided due to these photoprotective mechanisms. The lack of considering this plant acclimation strategy to low temperature occurring with already significant radiation leads to an overestimation of photosynthetic efficiency in models. This can further result in the overestimation of GPP in spring.

In this study, we did not disentangle the DSPR effects on GPP bias caused by photodamage vs photoprotection. As photoprotection is often achieved by the increase of photoprotective pigments such as carotenoids and specifically xanthophylls (VAZ, violaxanthin + antheraxanthin + zeaxanthin; Ensminger *et al.*, 2006; Verhoeven, 2014), seasonal changes in effects of photoprotection can be tracked through tracking these pigment pools size variation. Thanks to the fast development of remote sensing techniques in the past decades, it is now possible to monitor the pigments' variation in a nondestructive way through different vegetation indexes and at different spatial scales (Gamon *et al.*, 2016; D'Odorico *et al.*, 2020, 2021; Chen *et al.*, 2021; Yin *et al.*, 2022). One example is to use chlorophyll/carotenoid index (CCI) calculated through MODIS ocean bands on the ecosystem scale. In contrast, photodamage induces a swift browning of the canopy, specifically for deciduous trees, after frost events and is also detectable by vegetation indexes such as the enhanced vegetation index (EVI), or the green chromatic coordinate (GCC; Hufkens *et al.*, 2012). Making better use of the full spectral information in remotely sensed surface reflectance data may enable a better capturing of variations in photosynthetic and photoprotective pigments and plant stresses (Gamon *et al.*, 2016) and may enable a better detection of apparent DSPR effects on the ecosystem fluxes. Although photodamage could contribute to the DSPR identified here, we note that respective patterns were a regularly recurring phenomenon at affected sites. Therefore, the environmental stressor (high light and low temperature) is not rare (extreme) and it appears reasonable to hypothesize that plants are adapted to such conditions. Hence, we expect that the DSPR as identified here is mostly an expression of protection, not damage.

Apart from photodamage and photoprotection, hydraulic stress and/or damage from cold events on trees' water transport system can also result in a delayed resumption of GPP in temperate and boreal forests (Wang *et al.*, 1992; Cavender-Bares, 2005; Sims *et al.*, 2008). From the comparison of results between $SY_{DSPR}$ and $SY_0$ (Fig. 4), we can infer that soil temperature is not the main cause for DSPR. Since most of the sites in $SY_{DSPR}$ are covered by snow in the winter, the thermal insulation effects from the snow keep the soil temperature *c.* 0°C (Jungqvist *et al.*, 2014). This result is consistent with Bergh & Linder (1999), who found that the recovery of photosynthesis was mainly determined by air temperature rather than soil temperature. Soil moisture might be one reason that contributes to delayed recovery of photosynthesis in $SY_{DSPR}$. However, as soil moisture data in most of the sites are only available for the shallow layer, more sites with complete soil moisture at different soil depths are needed to further test this hypothesis. Based on the above-mentioned findings, we suggest conducting additional measurements on selected forest EC sites in boreal and temperate regions in future studies for a causal attribution of the DSPR phenomenon to particular processes and for discriminating

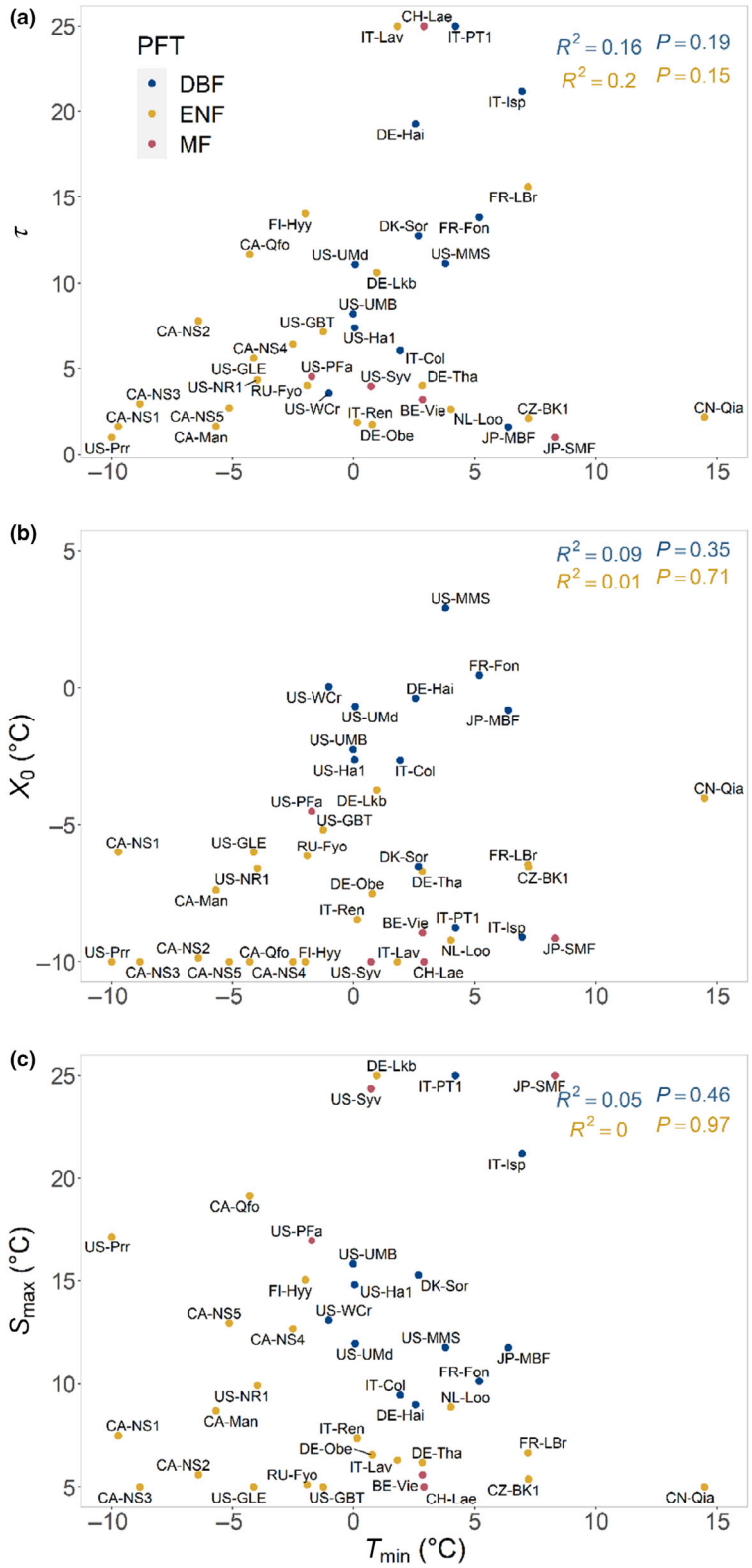


**Fig. 7** Calibrated parameters: (a) parameter $\tau$, (b) parameter $X_0$, and (c) parameter $S_{max}$ vs the minimum air temperature ($T_{min}$) during the period between 60 d before the start of photosynthesis resumption period and peak of the GPP at the site scale. The coefficient of determination ($R^2$) and $P$-values are shown for linear regressions between minimum temperature ($T_{min}$) and parameters. DBF, deciduous broadleaf forest; ENF, evergreen needleleaf forest; MF, mixed deciduous and evergreen needleleaf forest. For detailed definitions of different Köppen–Geiger climate zones (Clim) (Table 1). Two classes of sites (DBF (blue) and Dfc-ENF (orange)) were highlighted.

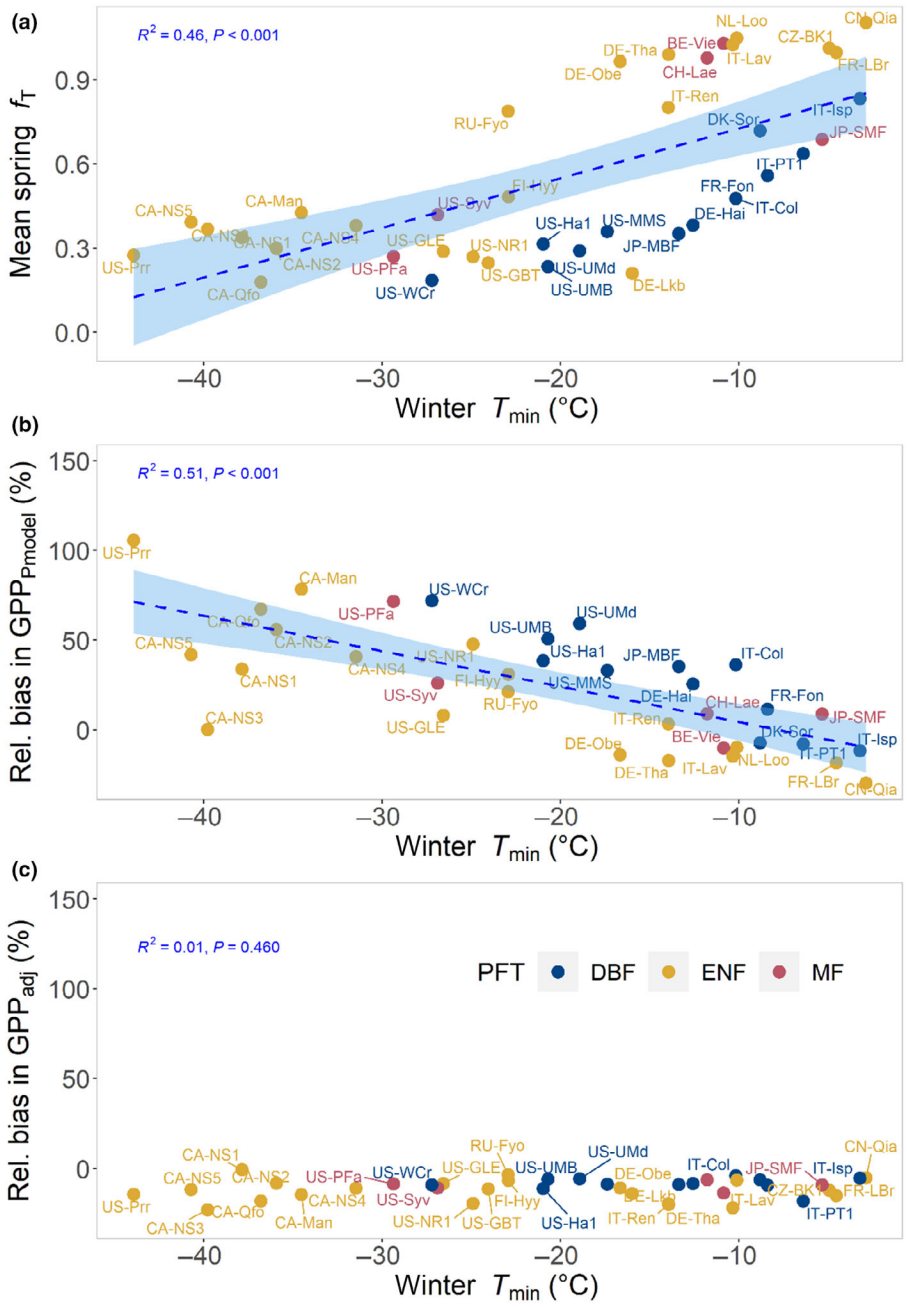


**Fig. 8** Relationship between minimum temperature ($T_{min}$) during winter and (a) mean spring cold-acclimated temperature modifier ($f_T$) or relative (Rel.) mean GPP bias before applying $f_T$ (b; $GPP_{Pmodel}$) and after applying $f_T$ (c; $GPP_{adj}$) among different sites. $GPP_{bias}$ is defined as GPP bias over observed GPP ($GPP_{obs}$). The colours indicate the plant function types (PFTs) of sites. Regression lines were added if the slope of linear regression is statistically significantly different from zero. DBF, deciduous broadleaf forest; ENF, evergreen needleleaf forest; MF, mixed deciduous and evergreen needleleaf forest; $R^2$, the coefficient of determination.

effects of protective vs damage. Measurements may comprise, for example multispectral drone-based remote sensing of canopy reflectance, measurements of hydraulic properties, including soil and leaf water potentials, and photosynthesis measurements.

## Considering delay effects of temperature improves GPP representation in cold regions

Results from our analysis with the LME and P-model (Fig. 1) indicated that only considering the effects of concurrent climate drivers on LUE is not sufficient to accurately model GPP. The reduced springtime LUE observed at most sites in winter-cold temperate and boreal ecosystems is governed by a delayed response of photosynthetic activity to springtime warming after low winter temperatures. This is most evident at sites located in North America and less evident for a few temperate European sites with modestly cold winters and springtime minimum temperatures (Figs 2, 8c).

By taking into account cold acclimation of photosynthesis and delayed effects of low temperatures in winter and early spring into the P-model, we largely reduced the early spring GPP overestimation bias. The MAE was reduced by 22% for pooled data from different sites and years during the photosynthesis resumption period. This bias reduction is most clearly evident for the sites and years with cold winters and early spring (Figs 5, 8). Previous studies have recognized the importance of a hysteretic

temperature effect for modelling photosynthesis of coniferous forests in boreal and temperate regions (Mäkelä *et al.*, 2004, 2008; Gea-Izquierdo *et al.*, 2010). For instance, after considering the lagged effect of low temperatures in a similar model, Gea-Izquierdo *et al.* (2010) found the model efficiency to have significantly improved.

Even though much less discussed compared with evergreens (van Dijk *et al.*, 2005; Tian *et al.*, 2020; Bao *et al.*, 2022b), here, we document substantial effects of DSPR also on deciduous vegetation as shown in Fig. 1. As discussed in 'The bias in springtime GPP simulations is due to neglected effects on photosynthesis' in the Discussion, the GPP overestimation in the early spring in DBF can be mainly attributed to the overestimated LUE (Figs 3, S5). The significant improvement of the GPP simulation for deciduous forests located in regions with cold winters (Dfb-DBF and Dfc-DBF) after embedding a delayed response to temperature in the model (Fig. 5) indicates the importance of delayed low-temperature delay effects for photosynthesis also in deciduous forests.

The delayed recovery of photosynthetic capacity and $CO_2$ assimilation in spring is also an adaptation mechanism of plants to escape the damage from potential frost events (Vitasse *et al.*, 2014; Liu *et al.*, 2018). In climates with low spring temperatures and with high spring temperature variability, and consequently a high probability of late frost events, plants tend to leaf-out late (specifically for deciduous trees forest) and at the same time deploy higher leaf freezing resistance (Zohner *et al.*, 2017). This results in a later recovery of photosynthetic activity compared with regions with mild temperature variability (Zohner *et al.*, 2017, 2020). For instance, Zohner *et al.* (2020) found Northern America to harbour in general tree species with a more cautious leaf-out strategy compared with Europe and East Asia, which is mainly due to the plants being exposed to higher interannual spring temperature variability there (Zohner *et al.*, 2017). This phenomenon is also consistent with our comparison between modelled and observed GPP (Figs 2, S3): most North American sites exhibit a distinct GPP overestimation in the spring, while the GPP overestimation is not evident for many sites in Europe, especially the sites located in regions with a maritime climate in western Europe.

### Implications for GPP projection under climate change

Over the past several decades, global warming and climate change have promoted earlier spring leaf unfolding (Menzel *et al.*, 2006; Fu *et al.*, 2015; Piao *et al.*, 2019) and a significant increase in vegetation greenness (Zhu *et al.*, 2016; Piao *et al.*, 2020), which enhances global terrestrial carbon uptake (Piao *et al.*, 2020). Global warming tends to continuously advance the leaf onset of deciduous forests and extend the growing season in temperate and boreal forests. However, the frequency of extreme weather events is also projected to increase (Marino *et al.*, 2011; Rahmstorf & Coumou, 2011), including an increase in late frost events that occur after leaf unfolding (Liu *et al.*, 2018), which can have a large impact on forest productivity (Gu *et al.*, 2008; Hufkens *et al.*, 2012). Currently, most state-of-the-art Earth System Models do not consider the potential impact of the increasing probability of frost events in the early (and advanced) growing season with global warming induced by the hysteretic recovery of photosynthesis after cold events. This implies that the projected global terrestrial carbon uptake might be overestimated (Liu *et al.*, 2018) in regions where cold winters and springs lead to a delayed springtime photosynthesis resumption. Accounting for the delayed effects of low temperature on photosynthesis as done in this study, combined with improved prognostic phenology representation in Dynamic Global Vegetation Models and Earth System models (Richardson *et al.*, 2012; Basler, 2016), could enable more accurate simulations of the land carbon uptake in northern ecosystems under future climate change and provide reliable estimates of carbon cycle impacts by springtime frost events.

## Acknowledgements

The authors acknowledge the internal project PhotoCold from the Swiss Federal Institute for Forest, Snow and Landscape Research WSL for supporting this research. Part of the work was funded by Velux Stiftung (Project No. 1734). BDS was funded by the Swiss National Science Foundation grant PCEFP2_181115. This work is a contribution to the LEMON-TREE (Land Ecosystem Models based On New Theory, obseRvations and ExperimEnts) project, funded through the generosity of Eric and Wendy Schmidt by recommendation of the Schmidt Futures programme (BDS). This work used eddy covariance data acquired and shared by the FLUXNET community, including these networks: AmeriFlux, AfriFlux, AsiaFlux, CarboAfrica, CarboEuropeIP, CarboItaly, CarboMont, ChinaFlux, Fluxnet-Canada, GreenGrass, ICOS, KoFlux, LBA, NECC, OzFlux-TERN, TCOS-Siberia, and USCCC. Open access funding provided by ETH-Bereich Forschungsanstalten.

## Competing interests

None declared.

## Author contributions

BDS, YL and AG designed the research. YL performed the research and analysed the data. BDS also contributed to part of the data analysis. PD and KH helped YL process the remote sensing data and the relevant interpretation. YL wrote the original manuscript. All authors contributed to the discussion of the results and substantial improvements in the writing of the manuscript.

## ORCID

Petra D'Odorico https://orcid.org/0000-0001-9954-8508
Arthur Gessler https://orcid.org/0000-0002-1910-9589
Yunpeng Luo https://orcid.org/0000-0001-6383-8300
Benjamin D. Stocker https://orcid.org/0000-0003-2697-9096

## Data availability

Code for the data analysis of this study is available at the GitHub repository: https://github.com/lypluo/photocold_manuscript. Modelled GPP from P-model at FLUXNET sites is available from Zendo (Stocker, 2019).

## References


**Acosta M, Pavelka M, Montagnani L, Kutsch W, Lindroth A, Juszczak R, Janouš D. 2013.** Soil surface $CO_2$ efflux measurements in Norway spruce forests: comparison between four different sites across Europe – from boreal to alpine forest. *Geoderma* **192**: 295–303.

**Bao S, Ibrom A, Wohlfahrt G, Koirala S, Migliavacca M, Zhang Q, Carvalhais N. 2022a.** Narrow but robust advantages in two-big-leaf light use efficiency models over big-leaf light use efficiency models at ecosystem level. *Agricultural and Forest Meteorology* **326**: 109185.

**Bao S, Wutzler T, Koirala S, Cuntz M, Ibrom A, Besnard S, Walther S, Šigut L, Moreno A, Weber U *et al.* 2022b.** Environment-sensitivity functions for gross primary productivity in light use efficiency models. *Agricultural and Forest Meteorology* **312**: 108708.

**Basler D. 2016.** Evaluating phenological models for the prediction of leaf-out dates in six temperate tree species across central Europe. *Agricultural and Forest Meteorology* **217**: 10–21.

**Bates D, Mächler M, Bolker B, Walker S. 2015.** Fitting linear mixed-effects models using LME4. *Journal of Statistical Software* **67**: 1–48.

**Beck HE, Zimmermann NE, McVicar TR, Vergopolan N, Berg A, Wood EF. 2018.** Present and future Köppen-Geiger climate classification maps at 1-km resolution. *Scientific Data* **5**: 180214.

**Berbigier P, Bonnefond J-M, Mellmann P. 2001.** $CO_2$ and water vapour fluxes for 2 years above Euroflux forest site. *Agricultural and Forest Meteorology* **108**: 183–197.

**Bergeron O, Margolis HA, Black TA, Coursolle C, Dunn AL, Barr AG, Wofsy SC. 2007.** Comparison of carbon dioxide fluxes over three boreal black spruce forests in Canada. *Global Change Biology* **13**: 89–107.

**Bergh J, Linder S. 1999.** Effects of soil warming during spring on photosynthetic recovery in boreal Norway spruce stands. *Global Change Biology* **5**: 245–253.

**Bergh J, McMurtrie RE, Linder S. 1998.** Climatic factors controlling the productivity of Norway spruce: a model-based analysis. *Forest Ecology and Management* **110**: 127–139.

**Bernacchi CJ, Pimentel C, Long SP. 2003.** *In vivo* temperature response functions of parameters required to model RuBP-limited photosynthesis. *Plant, Cell & Environment* **26**: 1419–1430.

**Bernhofer C, Grünwald T, Moderow U, Hehn M, Eichelmann U, Prasse H, Postel U. 2008–2014.** *FLUXNET2015 DE-Obe Oberbärenburg.* doi: 10.18140/FLX/1440151.

**Bloomfield KJ, Stocker BD, Keenan TF, Prentice IC. 2023.** Environmental controls on the light use efficiency of terrestrial gross primary production. *Global Change Biology* **29**: 1037–1053.

**Bradshaw CJA, Warkentin IG. 2015.** Global estimates of boreal forest carbon stocks and flux. *Global and Planetary Change* **128**: 24–30.

**von Caemmerer S, Farquhar GD. 1981.** Some relationships between the biochemistry of photosynthesis and the gas exchange of leaves. *Planta* **153**: 376–387.

**Cavender-Bares J. 2005.** Impacts of freezing on long distance transport in woody plants. In: Cavender-Bares J, ed. *Vascular transport in plants.* Amsterdam, Netherlands: Elsevier, 401–424.

**Chang CY-Y, Bräutigam K, Hüner NPA, Ensminger I. 2021.** Champions of winter survival: cold acclimation and molecular regulation of cold hardiness in evergreen conifers. *New Phytologist* **229**: 675–691.

**Charrier G, Martin-StPaul N, Damesin C, Delpierre N, Hänninen H, Torres-Ruiz JM, Davi H. 2021.** Interaction of drought and frost in tree ecophysiology: rethinking the timing of risks. *Annals of Forest Science* **78**: 40.

**Chen S, Kosugi Y, Jiao L, Nakaji T, Noda H, Hikosaka K, Nasahara K. 2021.** Winter leaf reddening phenomenon: the long-term track of PRI and phenological changes in a temperate Japanese cypress forest at Kiryu Japan. *EGU General Assembly Conference Abstracts.* EGU21-6849.

**Cheng Y, Gamon JA, Fuentes DA, Mao Z, Sims DA, Qiu H-L, Claudio H, Huete A, Rahman AF. 2006.** A multi-scale analysis of dynamic optical signals in a Southern California chaparral ecosystem: a comparison of field, AVIRIS and MODIS data. *Remote Sensing of Environment* **103**: 369–378.

**Cong N, Wang T, Nan H, Ma Y, Wang X, Myneni RB, Piao S. 2013.** Changes in satellite-derived spring vegetation green-up date and its linkage to climate in China from 1982 to 2010: a multimethod analysis. *Global Change Biology* **19**: 881–891.

**Cook BD, Davis KJ, Wang W, Desai A, Berger BW, Teclaw RM, Martin JG, Bolstad PV, Bakwin PS, Yi C *et al.* 2004.** Carbon exchange and venting anomalies in an upland deciduous forest in northern Wisconsin, USA. *Agricultural and Forest Meteorology* **126**: 271–295.

**Delpierre N, Berveiller D, Granda E, Dufrêne E. 2016.** Wood phenology, not carbon input, controls the interannual variability of wood growth in a temperate oak forest. *New Phytologist* **210**: 459–470.

**Demmig-Adams B, Adams WW. 1996.** The role of xanthophyll cycle carotenoids in the protection of photosynthesis. *Trends in Plant Science* **1**: 21–26.

**Desai AR, Bolstad PV, Cook BD, Davis KJ, Carey EV. 2005.** Comparing net ecosystem exchange of carbon dioxide between an old-growth and mature forest in the upper Midwest, USA. *Agricultural and Forest Meteorology* **128**: 33–55.

**Desai AR, Xu K, Tian H, Weishampel P, Thom J, Baumann D, Andrews AE, Cook BD, King JY, Kolka R. 2015.** Landscape-level terrestrial methane flux observed from a very tall tower. *Agricultural and Forest Meteorology* **201**: 61–75.

**van Dijk AIJM, Dolman AJ, Schulze E-D. 2005.** Radiation, temperature, and leaf area explain ecosystem carbon fluxes in boreal and temperate European forests. *Global Biogeochemical Cycles* **19**: 20–29.

**D'Odorico P, Besik A, Wong CYS, Isabel N, Ensminger I. 2020.** High-throughput drone-based remote sensing reliably tracks phenology in thousands of conifer seedlings. *New Phytologist* **226**: 1667–1681.

**D'Odorico P, Schönbeck L, Vitali V, Meusburger K, Schaub M, Ginzler C, Zweifel R, Velasco VME, Gisler J, Gessler A *et al.* 2021.** Drone-based physiological index reveals long-term acclimation and drought stress responses in trees. *Plant, Cell & Environment* **44**: 3552–3570.

**Dragoni D, Schmid HP, Wayson CA, Potter H, Grimmond CSB, Randolph JC. 2011.** Evidence of increased net ecosystem productivity associated with a longer vegetated season in a deciduous forest in south-central Indiana, USA. *Global Change Biology* **17**: 886–897.

**Dunn AL, Barford CC, Wofsy SC, Goulden ML, Daube BC. 2007.** A long-term record of carbon exchange in a boreal black spruce forest: means, responses to interannual variability, and decadal trends. *Global Change Biology* **13**: 577–590.

**Ensminger I, Busch F, Huner NPA. 2006.** Photostasis and cold acclimation: sensing low temperature through photosynthesis. *Physiologia Plantarum* **126**: 28–44.

**Ensminger I, Sveshnikov D, Campbell DA, Funk C, Jansson S, Lloyd J, Shibistova O, Öquist G. 2004.** Intermittent low temperatures constrain spring recovery of photosynthesis in boreal Scots pine forests. *Global Change Biology* **10**: 995–1008.

**Etzold S, Ruehr NK, Zweifel R, Dobbertin M, Zingg A, Pluess P, Häsler R, Eugster W, Buchmann N. 2011.** The carbon balance of two contrasting mountain forest ecosystems in Switzerland: similar annual trends, but seasonal differences. *Ecosystems* **14**: 1289–1309.

**Farquhar GD, von Caemmerer S, Berry JA. 1980.** A biochemical model of photosynthetic $CO_2$ assimilation in leaves of $C_3$ species. *Planta* **149**: 78–90.

**Ferréa C, Zenone T, Comolli R, Seufert G. 2012.** Estimating heterotrophic and autotrophic soil respiration in a semi-natural forest of Lombardy, Italy. *Pedobiologia* **55**: 285–294.

**Frank JM, Massman WJ, Ewers BE, Huckaby LS, Negrón JF. 2014.** Ecosystem $CO_2/H_2O$ fluxes are explained by hydraulically limited gas exchange during tree mortality from spruce bark beetles. *Journal of Geophysical Research: Biogeosciences* **119**: 1195–1215.

**Fu YH, Zhao H, Piao S, Peaucelle M, Peng S, Zhou G, Ciais P, Huang M, Menzel A, Peñuelas J *et al.* 2015.** Declining global warming effects on the phenology of spring leaf unfolding. *Nature* **526**: 104–107.

**Gamon JA, Huemmrich KF, Wong CYS, Ensminger I, Garrity S, Hollinger DY, Noormets A, Peñuelas J. 2016.** A remotely sensed pigment index reveals photosynthetic phenology in evergreen conifers. *Proceedings of the National Academy of Sciences, USA* **113**: 13087–13092.

**Gamon JA, Surfus JS. 1999.** Assessing leaf pigment content and activity with a reflectometer. *New Phytologist* **143**: 105–117.

**Gea-Izquierdo G, Mäkelä A, Margolis H, Bergeron Y, Black TA, Dunn A, Hadley J, Paw UKT, Falk M, Wharton S *et al.* 2010.** Modeling acclimation of photosynthesis to temperature in evergreen conifer forests. *New Phytologist* **188**: 175–186.

**Gough CM, Hardiman BS, Nave LE, Bohrer G, Maurer KD, Vogel CS, Nadelhoffer KJ, Curtis PS. 2013.** Sustained carbon uptake and storage following moderate disturbance in a Great Lakes forest. *Ecological Applications* **23**: 1202–1215.

**Goulden M. 2019.** *AmeriFlux BASE CA-NS1 UCI-1850 burn site, v.3-5.* AmeriFlux AMP. doi: 10.17190/AMF/1245999.

**Graven HD, Keeling RF, Piper SC, Patra PK, Stephens BB, Wofsy SC, Welp LR, Sweeney C, Tans PP, Kelley JJ *et al.* 2013.** Enhanced seasonal exchange of $CO_2$ by northern ecosystems since 1960. *Science* **341**: 1085–1089.

**Grünwald T, Bernhofer C. 2007.** A decade of carbon, water and energy flux measurements of an old spruce forest at the Anchor Station Tharandt. *Tellus B: Chemical and Physical Meteorology* **59**: 387–396.

**Gu L, Hanson PJ, Post WM, Kaiser DP, Yang B, Nemani R, Pallardy SG, Meyers T. 2008.** The 2007 eastern US spring freeze: increased cold damage in a warming world? *Bioscience* **58**: 253–262.

**Guo L, Gao J, Ma S, Chang Q, Zhang L, Wang S, Zou Y, Wu S, Xiao X. 2020.** Impact of spring phenology variation on GPP and its lag feedback for winter wheat over the North China Plain. *Science of the Total Environment* **725**: 138342.

**Hänninen H. 2016.** *Boreal and temperate trees in a changing climate.* Dordrecht, the Netherlands: Biometeorology, Springer.

**Haxeltine A, Prentice I. 1996.** A general model for the light-use efficiency of primary production. *Functional Ecology* **10**: 551–561.

**Holland MM, Bitz CM. 2003.** Polar amplification of climate change in coupled models. *Climate Dynamics* **21**: 221–232.

**Horn JE, Schulz K. 2011.** Identification of a general light use efficiency model for gross primary production. *Biogeosciences* **8**: 999–1021.

**Hufkens K. 2022.** *The MODISTOOLS package: an interface to the MODIS Land Products Subsets Web Services.* [WWW document] URL https://github.com/ropensci/MODISTools [accessed 20 August 2022].

**Hufkens K, Friedl MA, Keenan TF, Sonnentag O, Bailey A, O'Keefe J, Richardson AD. 2012.** Ecological impacts of a widespread frost event following early spring leaf-out. *Global Change Biology* **18**: 2365–2377.

**Huner NPA, Öquist G, Sarhan F. 1998.** Energy balance and acclimation to light and cold. *Trends in Plant Science* **3**: 224–230.

**Jiang C-D, Li P-M, Gao H-Y, Zou Q, Jiang G-M, Li L-H. 2005.** Enhanced photoprotection at the early stages of leaf expansion in field-grown soybean plants. *Plant Science* **168**: 911–919.

**Jungqvist G, Oni SK, Teutschbein C, Futter MN. 2014.** Effect of climate change on soil temperature in Swedish boreal forests. *PLoS ONE* **9**: e93957.

**Karageorgou P, Manetas Y. 2006.** The importance of being red when young: anthocyanins and the protection of young leaves of *Quercus coccifera* from insect herbivory and excess light. *Tree Physiology* **26**: 613–621.

**Keenan TF, Gray J, Friedl MA, Toomey M, Bohrer G, Hollinger DY, Munger JW, O'Keefe J, Schmid HP, Wing IS *et al.* 2014.** Net carbon uptake has increased through warming-induced changes in temperate forest phenology. *Nature Climate Change* **4**: 598–604.

**Keenan TF, Riley WJ. 2018.** Greening of the land surface in the world's cold regions consistent with recent warming. *Nature Climate Change* **8**: 825–828.

**Knohl A, Schulze E-D, Kolle O, Buchmann N. 2003.** Large carbon uptake by an unmanaged 250-year-old deciduous forest in Central Germany. *Agricultural and Forest Meteorology* **118**: 151–167.

**Kurbatova J, Li C, Varlagin A, Xiao X, Vygodskaya N. 2008.** Modeling carbon dynamics in two adjacent spruce forests with different soil conditions in Russia. *Biogeosciences* **5**: 969–980.

**Lindauer M, Schmid HP, Grote R, Mauder M, Steinbrecher R, Wolpert B. 2014.** Net ecosystem exchange over a non-cleared wind-throw-disturbed upland spruce forest – measurements and simulations. *Agricultural and Forest Meteorology* **197**: 219–234.

**Liu Q, Piao S, Janssens IA, Fu Y, Peng S, Lian X, Ciais P, Myneni RB, Peñuelas J, Wang T. 2018.** Extension of the growing season increases vegetation exposure to frost. *Nature Communications* **9**: 426.

**Luo Y, El-Madany TS, Filippa G, Ma X, Ahrens B, Carrara A, Gonzalez-Cascon R, Cremonese E, Galvagno M, Hammer TW *et al.* 2018.** Using near-infrared-enabled digital repeat photography to track structural and physiological phenology in Mediterranean tree–grass ecosystems. *Remote Sensing* **10**: 1293.

**Maire V, Martre P, Kattge J, Gastal F, Esser G, Fontaine S, Soussana J-F. 2012.** The coordination of leaf photosynthesis links C and N fluxes in $C_3$ plant species. *PLoS ONE* **7**: e38345.

**Mäkelä A, Hari P, Berninger F, Hänninen H, Nikinmaa E. 2004.** Acclimation of photosynthetic capacity in Scots pine to the annual cycle of temperature. *Tree Physiology* **24**: 369–376.

**Mäkelä A, Pulkkinen M, Kolari P, Lagergren F, Berbigier P, Lindroth A, Loustau D, Nikinmaa E, Vesala T, Hari P. 2008.** Developing an empirical model of stand GPP with the LUE approach: analysis of eddy covariance data at five contrasting conifer sites in Europe. *Global Change Biology* **14**: 92–108.

**Marcolla B, Pitacco A, Cescatti A. 2003.** Canopy architecture and turbulence structure in a coniferous forest. *Boundary-Layer Meteorology* **108**: 39–59.

**Marino GP, Kaiser DP, Gu L, Ricciuto DM. 2011.** Reconstruction of false spring occurrences over the southeastern United States, 1901–2007: an increasing risk of spring freeze damage? *Environmental Research Letters* **6**: 024015.

**Matsumoto K, Ohta T, Nakai T, Kuwada T, Daikoku K, Si I, Yabuki H, Kononov AV, van der Molen MK, Kodama Y *et al.* 2008.** Energy consumption and evapotranspiration at several boreal and temperate forests in the Far East. *Agricultural and Forest Meteorology* **148**: 1978–1989.

**Menzel A, Sparks TH, Estrella N, Koch E, Aasa A, Ahas R, Alm-Kübler K, Bissolli P, Braslavská OG, Briede A *et al.* 2006.** European phenological response to climate change matches the warming pattern. *Global Change Biology* **12**: 1969–1976.

**Migliavacca M, Galvagno M, Cremonese E, Rossini M, Meroni M, Sonnentag O, Cogliati S, Manca G, Diotri F, Busetto L *et al.* 2011.** Using digital repeat photography and eddy covariance data to model grassland phenology and photosynthetic $CO_2$ uptake. *Agricultural and Forest Meteorology* **151**: 1325–1337.

**Migliavacca M, Meroni M, Busetto L, Colombo R, Zenone T, Matteucci G, Manca G, Seufert G. 2009.** Modeling gross primary production of agro-forestry ecosystems by assimilation of satellite-derived information in a process-based model. *Sensors* **9**: 922–942.

**Monson RK, Turnipseed AA, Sparks JP, Harley PC, Scott-Denton LE, Sparks K, Huxman TE. 2002.** Carbon sequestration in a high-elevation, subalpine forest. *Global Change Biology* **8**: 459–478.

**Monteith J. 1972.** Solar radiation and productivity in tropical ecosystems. *Journal of Applied Ecology* **9**: 747–766.

**Moody EG, King MD, Schaaf CB, Hall DK, Platnick S. 2007.** Northern Hemisphere five-year average (2000–2004) spectral albedos of surfaces in the presence of snow: statistics computed from Terra MODIS land products. *Remote Sensing of Environment* **111**: 337–345.

**Moors EJ. 2012.** *Water use of forests in the Netherlands.* Vrije Universiteit. [WWW document] URL https://edepot.wur.nl/213926 [accessed 20 December 2021].

**Myneni R, Knyazikhin Y, Park T. 2015.** *MOD15A2H MODIS/Terra leaf area Index/FPAR 8-Day L4 global 500m SIN grid V006.* NASA EOSDIS Land Processes DAAC. [WWW document] URL https://ladsweb.modaps.eosdis.nasa.gov/missions-and-measurements/products/MOD15A2H [accessed 31 January 2022].

**Nakai T, Kim Y, Busey RC, Suzuki R, Nagai S, Kobayashi H, Park H, Sugiura K, Ito A. 2013.** Characteristics of evapotranspiration from a permafrost black spruce forest in interior Alaska. *Polar Science* **7**: 136–148.

**Ottander C, Campbell D, Öquist G. 1995.** Seasonal changes in photosystem II organisation and pigment composition in *Pinus sylvestris*. *Planta* **197**: 176–183.

**Pastorello G, Trotta C, Canfora E, Chu H, Christianson D, Cheah Y-W, Poindexter C, Chen J, Elbashandy A, Humphrey M *et al.* 2020.** The

FLUXNET2015 dataset and the ONEFlux processing pipeline for eddy covariance data. *Scientific Data* 7: 225.

**Piao S, Friedlingstein P, Ciais P, Viovy N, Demarty J. 2007.** Growing season extension and its impact on terrestrial carbon cycle in the Northern Hemisphere over the past 2 decades. *Global Biogeochemical Cycles* **21**: 1–15.

**Piao S, Liu Q, Chen A, Janssens IA, Fu Y, Dai J, Liu L, Lian X, Shen M, Zhu X. 2019.** Plant phenology and global climate change: current progresses and challenges. *Global Change Biology* **25**: 1922–1940.

**Piao S, Wang X, Park T, Chen C, Lian X, He Y, Bjerke JW, Chen A, Ciais P, Tømmervik H *et al.* 2020.** Characteristics, drivers and feedbacks of global greening. *Nature Reviews Earth & Environment* **1**: 14–27.

**Pilegaard K, Ibrom A, Courtney MS, Hummelshøj P, Jensen NO. 2011.** Increasing net $CO_2$ uptake by a Danish beech forest during the period from 1996 to 2009. *Agricultural and Forest Meteorology* **151**: 934–946.

**Prentice IC, Dong N, Gleason SM, Maire V, Wright IJ. 2014.** Balancing the costs of carbon gain and water transport: testing a new theoretical framework for plant functional ecology. *Ecology Letters* **17**: 82–91.

**Rahmstorf S, Coumou D. 2011.** Increase of extreme events in a warming world. *Proceedings of the National Academy of Sciences, USA* **108**: 17905–17909.

**Ranjan S, Singh R, Singh M, Pathre UV, Shirke PA. 2014.** Characterizing photoinhibition and photosynthesis in juvenile-red versus mature-green leaves of *Jatropha curcas* L. *Plant Physiology and Biochemistry* **79**: 48–59.

**Rantanen M, Karpechko AY, Lipponen A, Nordling K, Hyvärinen O, Ruosteenoja K, Vihma T, Laaksonen A. 2022.** The Arctic has warmed nearly four times faster than the globe since 1979. *Communications Earth & Environment* **3**: 168.

**Reichstein M, Falge E, Baldocchi D, Papale D, Aubinet M, Berbigier P, Bernhofer C, Buchmann N, Gilmanov T, Granier A *et al.* 2005.** On the separation of net ecosystem exchange into assimilation and ecosystem respiration: review and improved algorithm. *Global Change Biology* **11**: 1424–1439.

**Richardson AD, Anderson RS, Arain MA, Barr AG, Bohrer G, Chen G, Chen JM, Ciais P, Davis KJ, Desai AR *et al.* 2012.** Terrestrial biosphere models need better representation of vegetation phenology: results from the North American Carbon Program Site Synthesis. *Global Change Biology* **18**: 566–584.

**Rogers A, Medlyn BE, Dukes JS, Bonan G, von Caemmerer S, Dietze MC, Kattge J, Leakey ADB, Mercado LM, Niinemets Ü *et al.* 2017.** A roadmap for improving the representation of photosynthesis in Earth system models. *New Phytologist* **213**: 22–42.

**Rogers A, Serbin SP, Ely KS, Wullschleger SD. 2019.** Terrestrial biosphere models may overestimate Arctic $CO_2$ assimilation if they do not account for decreased quantum yield and convexity at low temperature. *New Phytologist* **223**: 167–179.

**Savage JA, Kiecker T, McMann N, Park D, Rothendler M, Mosher K. 2022.** Leaf out time correlates with wood anatomy across large geographic scales and within local communities. *New Phytologist* **235**: 953–964.

**Schaefer K, Schwalm CR, Williams C, Arain MA, Barr A, Chen JM, Davis KJ, Dimitrov D, Hilton TW, Hollinger DY *et al.* 2012.** A model-data comparison of gross primary productivity: results from the North American Carbon Program site synthesis. *Journal of Geophysical Research: Biogeosciences* **117**: 110–125.

**Shi M, Parazoo NC, Jeong S-J, Birch L, Lawrence P, Euskirchen ES, Miller CE. 2020.** Exposure to cold temperature affects the spring phenology of Alaskan deciduous vegetation types. *Environmental Research Letters* **15**: 025006.

**Sims DA, Rahman AF, Cordova VD, El-Masri BZ, Baldocchi DD, Bolstad PV, Flanagan LB, Goldstein AH, Hollinger DY, Misson L *et al.* 2008.** A new model of gross primary productivity for North American ecosystems based solely on the enhanced vegetation index and land surface temperature from MODIS. *Remote Sensing of Environment* **112**: 1633–1646.

**Singsaas EL, Ort DR, DeLucia EH. 2001.** Variation in measured values of photosynthetic quantum yield in ecophysiological studies. *Oecologia* **128**: 15–23.

**Stocker B. 2022.** *Ingest site-scale time series of environmental data from large files and remote repositories.* [WWW document] URL https://github.com/computationales/ingestr [accessed 13 March 2022].

**Stocker BD. 2019.** GPP at FLUXNET Tier 1 sites from P-model (v.2) [Data set]. *Zenodo*. doi: 10.5281/zenodo.3559850.

**Stocker BD, Wang H, Smith NG, Harrison SP, Keenan TF, Sandoval D, Davis T, Prentice IC. 2020.** P-model v.1.0: an optimality-based light use efficiency model for simulating ecosystem gross primary production. *Geoscientific Model Development* **13**: 1545–1581.

**Suni T, Rinne J, Reissell A, Altimir N, Keronen P, Rannik U, Maso M, Kulmala M, Vesala T. 2003.** Long-term measurements of surface fluxes above a Scots pine forest in Hyytiala, southern Finland, 1996-2001. *Boreal Environment Research* **8**: 287–302.

**Takahashi S, Badger MR. 2011.** Photoprotection in plants: a new light on photosystem II damage. *Trends in Plant Science* **16**: 53–60.

**Thomas SC. 2010.** Photosynthetic capacity peaks at intermediate size in temperate deciduous trees. *Tree Physiology* **30**: 555–573.

**Thurner M, Beer C, Santoro M, Carvalhais N, Wutzler T, Schepaschenko D, Shvidenko A, Kompter E, Ahrens B, Levick SR *et al.* 2014.** Carbon stock and density of northern boreal and temperate forests. *Global Ecology and Biogeography* **23**: 297–310.

**Tian X, Minunno F, Cao T, Peltoniemi M, Kalliokoski T, Mäkelä A. 2020.** Extending the range of applicability of the semi-empirical ecosystem flux model PRELES for varying forest types and climate. *Global Change Biology* **26**: 2923–2943.

**Tian X, Minunno F, Schiestl-Aalto P, Chi J, Zhao P, Peichl M, Marshall J, Näsholm T, Lim H, Peltoniemi M *et al.* 2021.** Disaggregating the effects of nitrogen addition on gross primary production in a boreal Scots pine forest. *Agricultural and Forest Meteorology* **301–302**: 108337.

**Toomey M, Friedl MA, Frolking S, Hufkens K, Klosterman S, Sonnentag O, Baldocchi DD, Bernacchi CJ, Biraud SC, Bohrer G *et al.* 2015.** Greenness indices from digital cameras predict the timing and seasonal dynamics of canopy-scale photosynthesis. *Ecological Applications* **25**: 99–115.

**Urbanski S, Barford C, Wofsy S, Kucharik C, Pyle E, Budney J, McKain K, Fitzjarrald D, Czikowsky M, Munger JW. 2007.** Factors controlling $CO_2$ exchange on timescales from hourly to decadal at Harvard Forest. *Journal of Geophysical Research: Biogeosciences* **112**: 169–194.

**Valentini R, De Angelis P, Matteucci G, Monaco R, Dore S, Mucnozza GES. 1996.** Seasonal net carbon dioxide exchange of a beech forest with the atmosphere. *Global Change Biology* **2**: 199–207.

**Vass I. 2012.** Molecular mechanisms of photodamage in the photosystem II complex. *Biochimica et Biophysica Acta (BBA) – Bioenergetics* **1817**: 209–217.

**Verhoeven A. 2014.** Sustained energy dissipation in winter evergreens. *New Phytologist* **201**: 57–65.

**Vitasse Y, Lenz A, Körner C. 2014.** The interaction between freezing tolerance and phenology in temperate deciduous trees. *Frontiers in Plant Science* **5**: 541.

**Walther S, Voigt M, Thum T, Gonsamo A, Zhang Y, Köhler P, Jung M, Varlagin A, Guanter L. 2016.** Satellite chlorophyll fluorescence measurements reveal large-scale decoupling of photosynthesis and greenness dynamics in boreal evergreen forests. *Global Change Biology* **22**: 2979–2996.

**Wang H, Prentice IC, Keenan TF, Davis TW, Wright IJ, Cornwell WK, Evans BJ, Peng C. 2017.** Towards a universal model for carbon dioxide uptake by plants. *Nature Plants* **3**: 734–741.

**Wang J, Ives NE, Lechowicz MJ. 1992.** The relation of foliar phenology to xylem embolism in trees. *Functional Ecology* **6**: 469–475.

**Wang YP, Leuning R. 1998.** A two-leaf model for canopy conductance, photosynthesis and partitioning of available energy I: model description and comparison with a multi-layered model. *Agricultural and Forest Meteorology* **91**: 89–111.

**Wen XF, Wang HM, Wang JL, Yu GR, Sun XM. 2010.** Ecosystem carbon exchanges of a subtropical evergreen coniferous plantation subjected to seasonal drought, 2003–2007. *Biogeosciences* **7**: 357–369.

**Xiang Y, Gubian S, Suomela B, Hoeng J. 2013.** Generalized simulated annealing for global optimization: the GENSA package. *R Journal* **5**: 13.

**Yang Q, Blanco NE, Hermida-Carrera C, Lehotai N, Hurry V, Strand Å. 2020.** Two dominant boreal conifers use contrasting mechanisms to reactivate photosynthesis in the spring. *Nature Communications* **11**: 128.

**Yin G, Verger A, Descals A, Filella I, Peñuelas J. 2022.** A broadband green-red vegetation index for monitoring gross primary production phenology. *Journal of Remote Sensing* **2022**: 9764982.

**Zarter CR, Adams WW III, Ebbert V, Cuthbertson DJ, Adamska I, Demmig-Adams B. 2006.** Winter down-regulation of intrinsic photosynthetic capacity coupled with up-regulation of Elip-like proteins and persistent energy dissipation in a subalpine forest. *New Phytologist* **172**: 272–282.

**Zeller KF, Nikolov NT. 2000.** Quantifying simultaneous fluxes of ozone, carbon dioxide and water vapor above a subalpine forest ecosystem. *Environmental Pollution* **107**: 1–20.

**Zhang Q. 2021.** Characterization of a seasonally snow-covered evergreen forest ecosystem. *International Journal of Applied Earth Observation and Geoinformation* **103**: 102464.

**Zhang Q, Xiao X, Braswell B, Linder E, Ollinger S, Smith M-L, Jenkins JP, Baret F, Richardson AD, Moore B III. 2006.** Characterization of seasonal variation of forest canopy in a temperate deciduous broadleaf forest, using daily MODIS data. *Remote Sensing of Environment* **105**: 189–203.

**Zhang Q, Yao T, Huemmrich KF, Middleton EM, Lyapustin A, Wang Y. 2020.** Evaluating impacts of snow, surface water, soil and vegetation on empirical vegetation and snow indices for the Utqiaġvik tundra ecosystem in Alaska with the LVS3 model. *Remote Sensing of Environment* **240**: 111677.

**Zhu Z, Piao S, Myneni RB, Huang M, Zeng Z, Canadell JG, Ciais P, Sitch S, Friedlingstein P, Arneth A *et al.* 2016.** Greening of the Earth and its drivers. *Nature Climate Change* **6**: 791–795.

**Zohner CM, Benito BM, Fridley JD, Svenning J-C, Renner SS. 2017.** Spring predictability explains different leaf-out strategies in the woody floras of North America, Europe and East Asia. *Ecology Letters* **20**: 452–460.

**Zohner CM, Mo L, Renner SS, Svenning J-C, Vitasse Y, Benito BM, Ordonez A, Baumgarten F, Bastin J-F, Sebald V *et al.* 2020.** Late-spring frost risk between 1959 and 2017 decreased in North America but increased in Europe and Asia. *Proceedings of the National Academy of Sciences, USA* **117**: 12192–12200.

## Supporting Information

Additional Supporting Information may be found online in the Supporting Information section at the end of the article.

**Fig. S1** Site location for the sites selected for the analysis.

**Fig. S2** Phenophases defined based on normalized time series of GPP.

**Fig. S3** Comparison of seasonal GPP from different data sources in each EC site.

**Fig. S4** Comparison of the mean seasonal cycle of light use efficiency (LUE) among different data sources.

**Fig. S5** Bias in GPP simulated by the linear mixed-effects regression LUE (LME) model within fAPAR bins and separated into the early and late seasons of northern ecosystems.

**Fig. S6** Distribution of residuals of observed vs modelled GPP, separated by fAPAR bins and by season in deciduous broadleaf forests.

**Fig. S7** Distribution of residuals of observed vs modelled GPP, separated by fAPAR bins and by season in evergreen needleleaf forests.

**Fig. S8** Comparison of daily fraction of absorbed photosynthetically active radiation (fAPAR) and snow fraction between the sites and years exhibiting a delayed springtime photosynthetic resumption (DSPR; $SY_{DSPR}$) and the sites and years were not affected by DSPR ($SY_0$).

**Fig. S9** Comparison of minimum air temperature ($T_{min}$) between the sites and years exhibiting a delayed springtime photosynthetic resumption (DSPR; $SY_{DSPR}$) and the sites and years that were not affected by DSPR ($SY_0$) under different bins of photosynthetically active radiation (PAR) at midday (10–14 h).

**Fig. S10** Comparison of minimum air temperature ($T_{min}$) between the sites and years exhibiting a delayed springtime photosynthetic resumption (DSPR; $SY_{DSPR}$) and the sites and years that were not affected by DSPR ($SY_0$) under shortwave incoming radiation ($SW_{IN}$) at midday (10–14 h).

**Fig. S11** Model evaluation after the cold-acclimation temperature modifier was applied to P-model, with its parameters optimized on the different scales.

**Fig. S12** Comparison of the mean seasonal cycle of GPP from different data sources (modelled GPP with site-specific parameters).

**Fig. S13** Comparison of the mean seasonal cycle of GPP from different data sources (modelled GPP with one general set of parameters).

**Notes S1** Alternative approach to embedding cold-acclimated modifier to reduce spring GPP bias.

Please note: Wiley is not responsible for the content or functionality of any Supporting Information supplied by the authors. Any queries (other than missing material) should be directed to the *New Phytologist* Central Office.